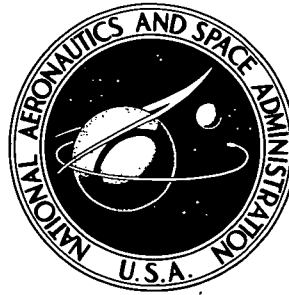


N 73-28693

NASA TECHNICAL NOTE



NASA TN D-7353

NASA TN D-7353

CASE FILE COPY

CHARACTERISTICS AND PERFORMANCE OF A SUPERCONDUCTING BUMPY-TORUS MAGNETIC FACILITY FOR PLASMA RESEARCH

*by J. Reece Roth, A. David Holmes, Thomas A. Keller,
and Walter M. Krawczonek*

*Lewis Research Center
Cleveland, Ohio 44135*

1. Report No. NASA TN D-7353		2. Government Accession No.		3. Recipient's Catalog No.	
4. Title and Subtitle CHARACTERISTICS AND PERFORMANCE OF A SUPER- CONDUCTING BUMPY-TORUS MAGNET FACILITY FOR PLASMA RESEARCH				5. Report Date August 1973	
				6. Performing Organization Code	
7. Author(s) J. Reece Roth, A. David Holmes, Thomas A. Keller, and Walter M. Krawczonek				8. Performing Organization Report No. E-7225	
9. Performing Organization Name and Address Lewis Research Center National Aeronautics and Space Administration Cleveland, Ohio 44135				10. Work Unit No. 503-10	
				11. Contract or Grant No.	
12. Sponsoring Agency Name and Address National Aeronautics and Space Administration Washington, D.C. 20546				13. Type of Report and Period Covered Technical Note	
				14. Sponsoring Agency Code	
15. Supplementary Notes					
16. Abstract The NASA Lewis bumpy-torus facility consists of 12 superconducting coils, each 19 cm i.d. and capable of 3.0 T on its axis. The coils are equally spaced around a toroidal array with a major diameter of 1.52 m; they are mounted with the major axis of the torus vertical in a single vacuum tank 2.6 m in diameter. Tests of the facility mapped out its magnetic, cryogenic, vacuum, mechanical, and electrical performance. The design value of the maximum magnetic field on the magnetic axis, 3.0 T, has been reached and exceeded. A maximum magnetic field of 3.23 T has been held for a period of 60 minutes. When the coils were charged to a maximum magnetic field of 3.35 T, the coil system went normal without apparent damage or degradation of performance.					
17. Key Words (Suggested by Author(s)) Superconductivity; Superconducting magnet; Toroidal magnetic field; Bumpy torus; Super- conducting magnetic facility; Fusion research; Plasma confinement				18. Distribution Statement Unclassified - unlimited	
19. Security Classif. (of this report) Unclassified		20. Security Classif. (of this page) Unclassified		21. No. of Pages 57	
				22. Price* \$3.00	

CONTENTS

	Page
SUMMARY	1
INTRODUCTION	2
DESIGN GOALS	5
FACILITY DESIGN	6
Superconducting Coil Design	6
Mechanical Design	17
Cryogenic System Design	20
Vacuum System Design	25
Instrumentation and Electrical Design	29
FACILITY APPEARANCE	39
FACILITY PERFORMANCE	43
Superconducting Coil Performance	43
Mechanical Performance	44
Cryogenic System Performance	49
Vacuum System Performance	52
Performance of Instrumentation and Electrical Systems	53
REFERENCES	54

CHARACTERISTICS AND PERFORMANCE OF A SUPERCONDUCTING BUMPY-TORUS MAGNETIC FACILITY FOR PLASMA RESEARCH

by J. Reece Roth, A. David Holmes, Thomas A. Keller
and Walter M. Krawczonek

Lewis Research Center

SUMMARY

This report presents data on the mechanical, electrical, cryogenic, and magnetic design and performance of the superconducting NASA Lewis "bumpy torus" magnetic facility. The phenomena observed and results obtained in plasma physics investigations in this facility are not discussed. The NASA Lewis superconducting bumpy-torus magnet facility contains 12 coils, each 19 centimeters in inside diameter and capable of 3.0 teslas on their axes, equally spaced in a toroidal array 1.52 meters in diameter. The coil array is mounted in a vacuum tank 2.6 meters in diameter. The 12 coils are electrically connected in series through the lower liquid-helium header and have a designed maximum magnetic field on the magnetic axis of 3.0 teslas. Five coils are wound with 2.16-millimeter (85-mil) diameter round conductor consisting of approximately 130 twisted niobium titanium (NbTi) filaments in a copper matrix. The remaining seven coils are wound of 2.03-millimeter (80-mil) square conductor consisting of approximately 14 untwisted NbTi filaments in a copper matrix. All 12 coils individually achieved their design current of 700 amperes and a centerpoint field of 3.0 teslas.

A maximum magnetic field on the magnetic axis of 3.0 teslas has been reached and held constant for periods in excess of 2 hours. A maximum magnetic field of 3.23 teslas has been held for a period of more than 60 minutes without a coil normalcy. The steady-state liquid-helium boiloff rate was 0.087 cubic meter (87 liters) per hour of liquid helium without the coils charged. The coil array showed no tendency toward mechanical instability when subjected to an impulsive loading, even with the magnets fully charged. When the coils were charged to a maximum magnetic field of 3.35 teslas, the system was driven normal without apparent damage to the facility or degradation of coil performance. At the present writing, the facility has experienced 24 normalcies without apparent damage to the magnet system.

INTRODUCTION

A modest research program is underway at the NASA Lewis Research Center to investigate the problems of ion heating, high-temperature plasma physics, and thermonuclear power production which are associated with space applications (refs. 1 and 2). The experimental apparatus described in this report was built at the NASA Lewis Research Center as one means to explore these and other space-related problems of plasma heating and confinement.

The "bumpy torus" magnetic field configuration receives its name from the shape assumed by a plasma confined in this geometry. Figure 1 shows a plasma confined in an axisymmetric mirror machine (the pilot-rig facility); the "bump" can be observed in the midplane where the magnetic field is weakest, and a necking down of the plasma in the regions of stronger field under the two coils at either side. A bumpy torus consists of a number of coils (12 for the Lewis facility) arranged as indicated in figure 2. The plasma assumes the form of a toroidal ring, with bumps in the region of weak field between the coils.

Many of the design features of the NASA Lewis bumpy torus facility were the result of experience gained with the superconducting pilot-rig facility, which consists of two coils and has been discussed in reference 3. An external view of the facility is shown in figure 3, and an isometric cutaway drawing of its coils and Dewars is shown in figure 4.

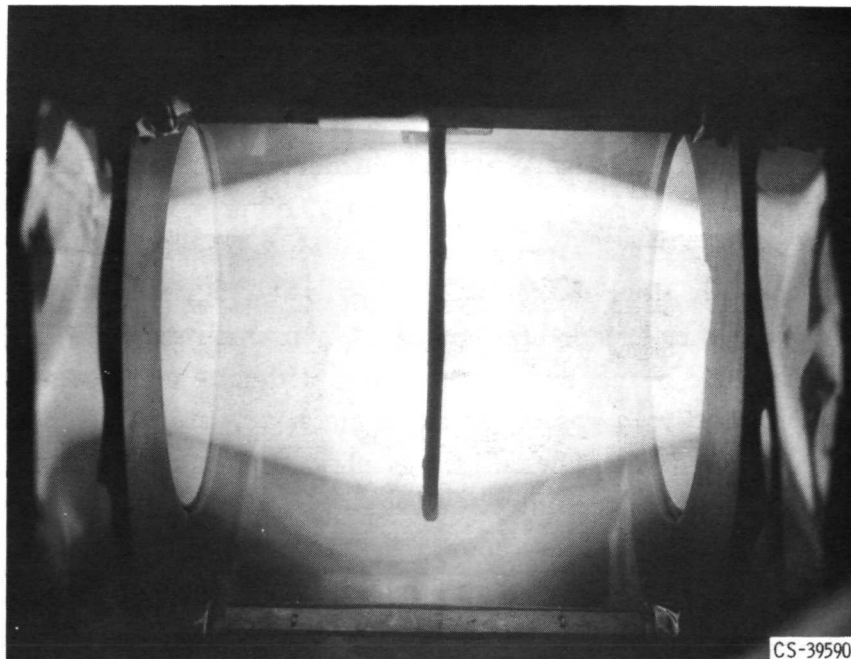


Figure 1. - Plasma in the pilot rig. Vertical element in center in a 16-centimeter-inner-diameter anode ring which is normally maintained at positive potentials of several tens of kilovolts.

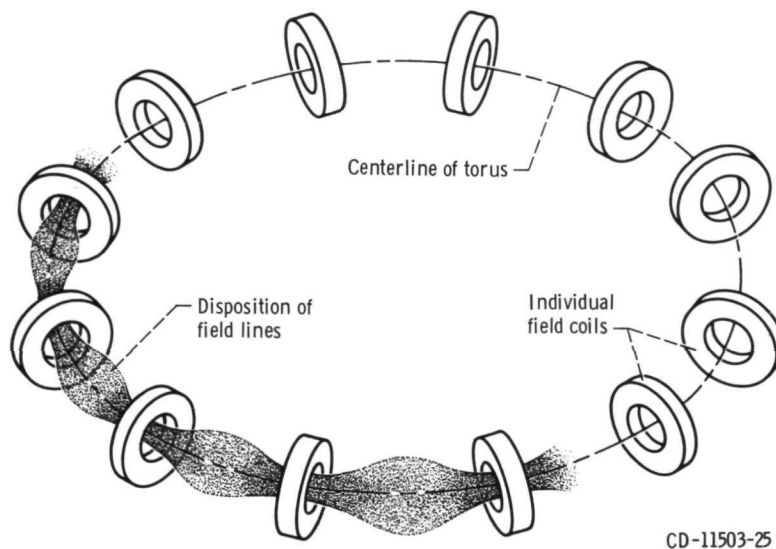


Figure 2. - Schematic drawing of bumpy-torus concept. Twelve superconducting magnets are arranged so that the plasma forms a toroidal volume.

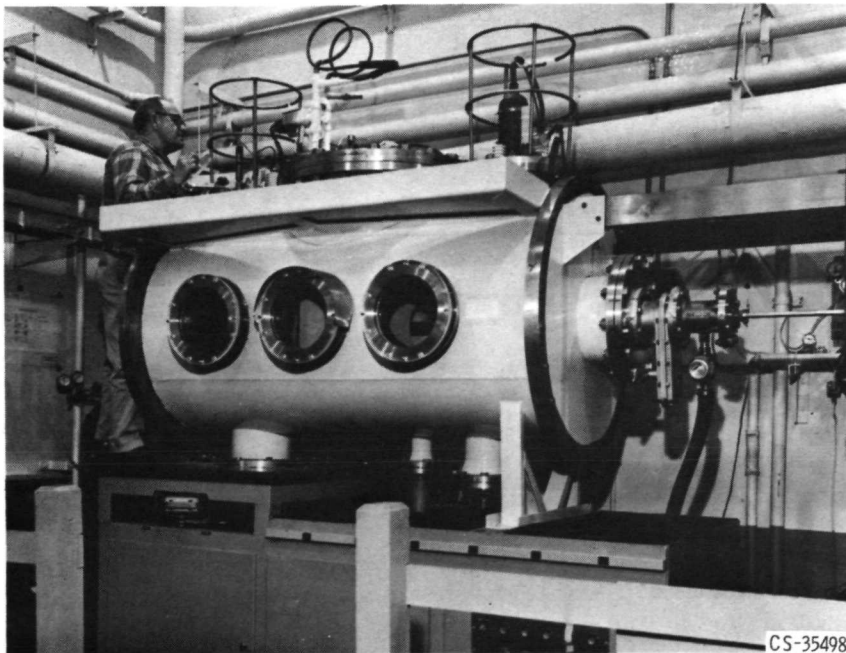


Figure 3. - 1-Meter-diameter, 2-meter-long vacuum tank of the pilot-rig magnetic facility.

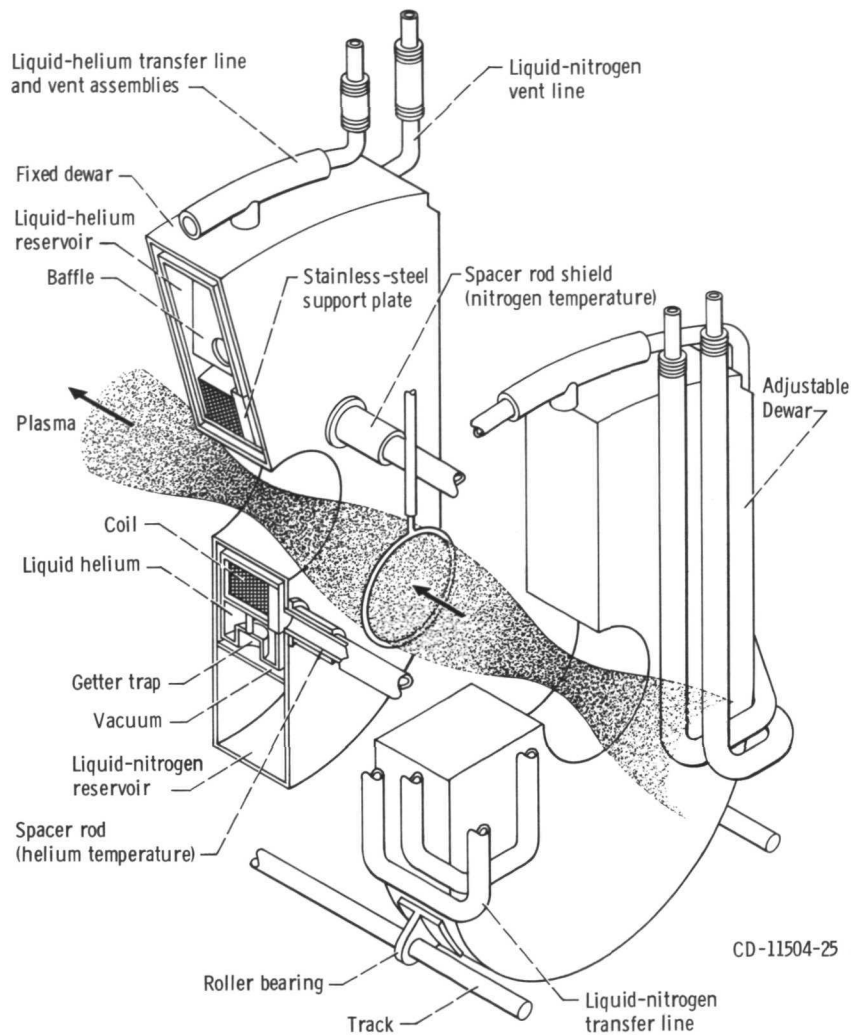


Figure 4. - Isometric cutaway drawing of two coil Dewars in the pilot rig.

The pilot rig first went into service on December 2, 1964, and is the first and longest operating superconducting magnet facility used in plasma physics and controlled-fusion research. In the period of 8 years ending December 31, 1972, the pilot rig experienced 584 liquid-helium loadings, approximately 60 percent of which represented thermal cycling between room temperature and liquid-helium temperature and approximately 40 percent of which represented thermal cycling between liquid-nitrogen temperature and liquid-helium temperature. Over the 8-year period there were 550 experimental runs with the magnets charged and 113 coil normalcies.

DESIGN GOALS

The plasma generated in the pilot rig, shown in figure 1, exceeded initial expectations so far as the heating of the plasma was concerned. Hot, Maxwellianized ions with kinetic temperatures as high as 7000 electron volts were observed in the pilot rig. At the same time that energy was transferred from the power supply to the ions, the electron temperatures were relatively low, no more than 100 to 200 electron volts. From a plasma physics point of view, the main defect of the magnetic field configuration of the pilot rig was that ions were lost rapidly, along the magnetic field lines to the end walls of the vacuum system at the right and left of figure 1. Although steady-state neutron production was observed in the pilot rig, it became clear that significant advances in ion density and containment time required the elimination of end losses of ions.

In reference 4 it was proposed to employ the bumpy-torus concept shown in figure 2, consisting of 12 superconducting magnetic field coils arranged in a toroidal array. The ions which would be lost to the vacuum-tank end walls are constrained by the magnetic field lines to circulate around the major circumference of the torus. It is anticipated that the reduction of end losses associated with the pilot-rig magnetic mirror geometry will permit higher particle densities and confinement times to be achieved in the bumpy-torus facility.

The number of field coils, the major and minor diameters of the toroidal array, and the design magnetic field strength were the result of an economic optimization described in reference 5. The major characteristics of the bumpy-torus geometry are listed in table I and result from maximizing the volume of confined plasma per dollar, subject to the constraint of adiabatic confinement of 10-keV deuterium ions.

Features of the pilot rig which proved troublesome in operation were avoided in the bumpy-torus facility. The inflexibility of the all-welded construction of the liquid-helium and liquid-nitrogen systems in the pilot rig was dealt with by putting Army-Navy (AN) fittings at appropriate locations, so that the 12 coils and their liquid-nitrogen shields could be separately removed from the facility when this became necessary or desirable. Another constraint was the necessity for simplicity and economy of construction. This

TABLE I. - DESIGN CHARACTERISTICS OF BUMPY-TORUS MAGNETIC FACILITY

Major diameter of torus, m	1.52
Inside diameter of spoolpiece, cm	21.0
Inside diameter of coil winding, cm	21.8
Outside diameter of coil winding, cm	30.5
Axial width of coil windings, cm	12.0
Design current for individual coil, A	700
Maximum magnetic field on axis of single coil at 700-A design current, T	3.00
Maximum magnetic field on magnetic axis of entire toroidal array, T	3.00
Mirror ratio on magnetic axis	2.48:1

dictated the use of sheet metal and silver solder joints, instead of a more elaborate construction involving machined parts or welded construction. The delay associated with the thermal inertia of the system was accepted, and the facility was designed so it could be operated for long periods with the magnets at cryogenic temperatures. For this reason, the 12 anode rings and all the experimental diagnostic equipment were designed to be inserted and withdrawn through airlocks on the vacuum tank.

The superconducting coils of the pilot rig were initially equipped with persistent switches, which consisted of 0.254-millimeter (10-mil) niobium zirconium (NbZr) wire wrapped around a 2-watt carbon resistor. One of the two persistent switches used failed; it is shown in figure 5. The failure indicated that the use of persistent switches, of the design used in the pilot rig, would be unwise in a facility containing 12 superconducting magnets.

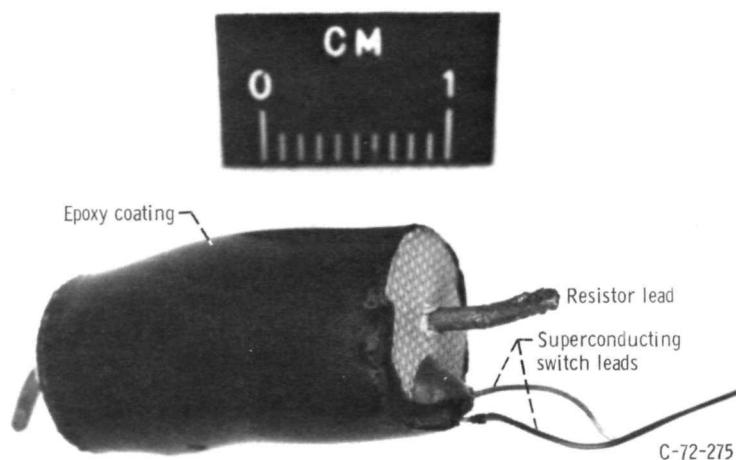


Figure 5. - Persistent switch from one of two pilot-rig superconducting coils.

FACILITY DESIGN

Superconducting Coil Design

A detailed design of the 12 individual coils was undertaken when the overall characteristics of the bumpy torus were determined. The 12 coils are virtually identical in their geometry and number of turns. The coil design was arrived at with the assistance of members of the Lewis staff. Similar work is described in references 6 and 7.

The coils were initially designed to use available square, untwisted NbTi superconducting wire. A transverse cross section of the square wire is shown in figure 6. This material has approximately 14 strands of superconducting material with a copper-to-

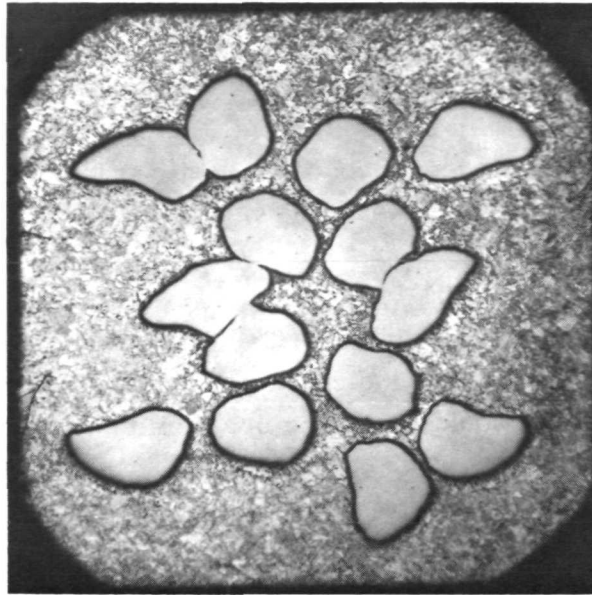
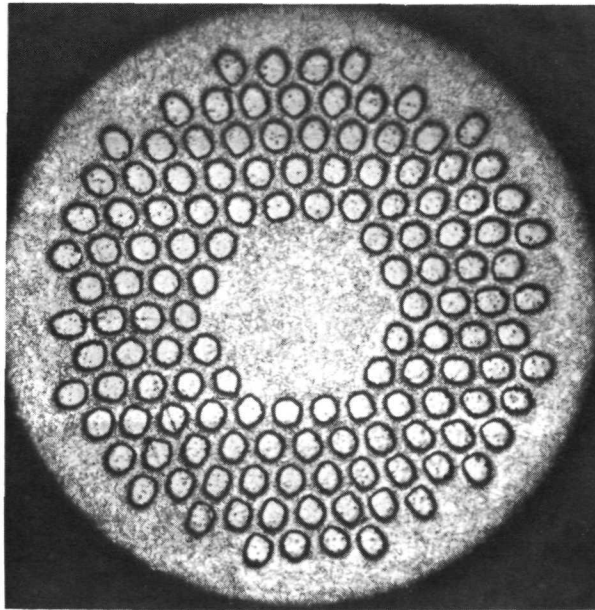


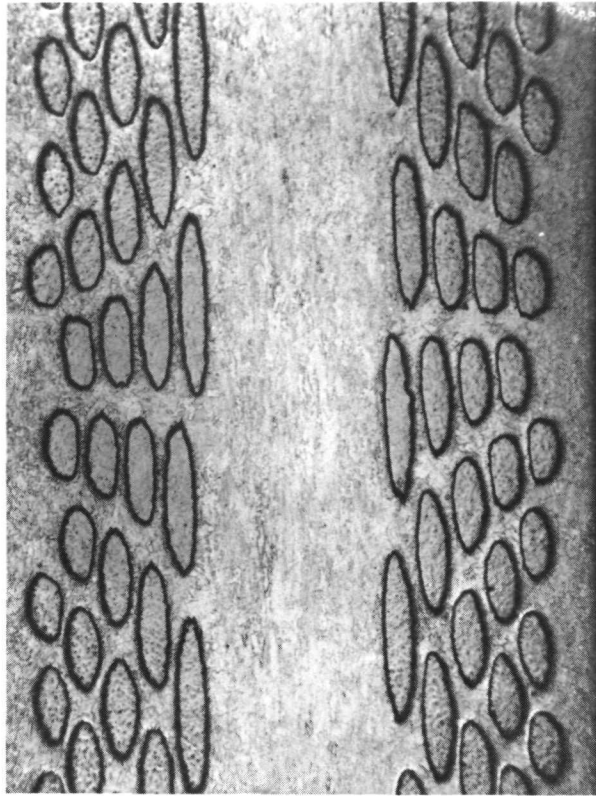
Figure 6. - Transverse cross section of square superconducting wire used in seven of the 12 coils of the bumpy torus facility, showing individual strands of superconducting wire imbedded in the copper matrix.

superconducting area ratio of 3.07. The wire is 2.03 millimeters (80 mils) square. The more or less random placement of the superconducting strands in the copper matrix was typical of this wire. At the time these coils were designed, it was recognized that wire which contained superconducting strands that were twisted about the longitudinal axis was preferable from a performance point of view. However, it was decided for economic reasons to use up the available untwisted square wire. In the final event, seven of the 12 coils were wound with the square, untwisted superconducting wire shown in figure 6; and five of the 12 coils were wound with the round, twisted superconducting wire shown in figure 7. This round wire has approximately 130 strands of NbTi superconducting wire embedded in a copper matrix with a copper-to-superconductor area ratio of 2.5. The very regular placement of the superconducting strands in the copper matrix is typical of this wire. The diameter of this wire is 2.16 millimeters (85 mils), and the wire is coated with a layer of insulating oxide. Figure 7(a) shows a transverse cross section. The twisting, spiral pattern of the superconducting strands in this wire is evident in the longitudinal cross section shown in figure 7(b).

The configuration of the cooling passages, the dimensions of the coil, and the relation of the windings to the spoolpiece are shown in figure 8. The windings are not drawn to scale. There are 18 layers from the inner to the outer radius of the windings and approximately 54 turns per layer. The individual turns of a given layer of the square wire are spaced apart by intermittent tabs of Mylar tape, which adheres to one face of the square wire. The Mylar tape tabs are 2.03 millimeters wide and approximately 12.7



(a) Transverse cross section of round wire, showing individual strands of superconducting wire imbedded in the copper matrix.



(b) Longitudinal cross section of round wire, showing helical twisting of the superconducting strands about wire axis.

Figure 7. - Cross sections of round wire used in five of the 12 coils of the bumpy-torus facility.

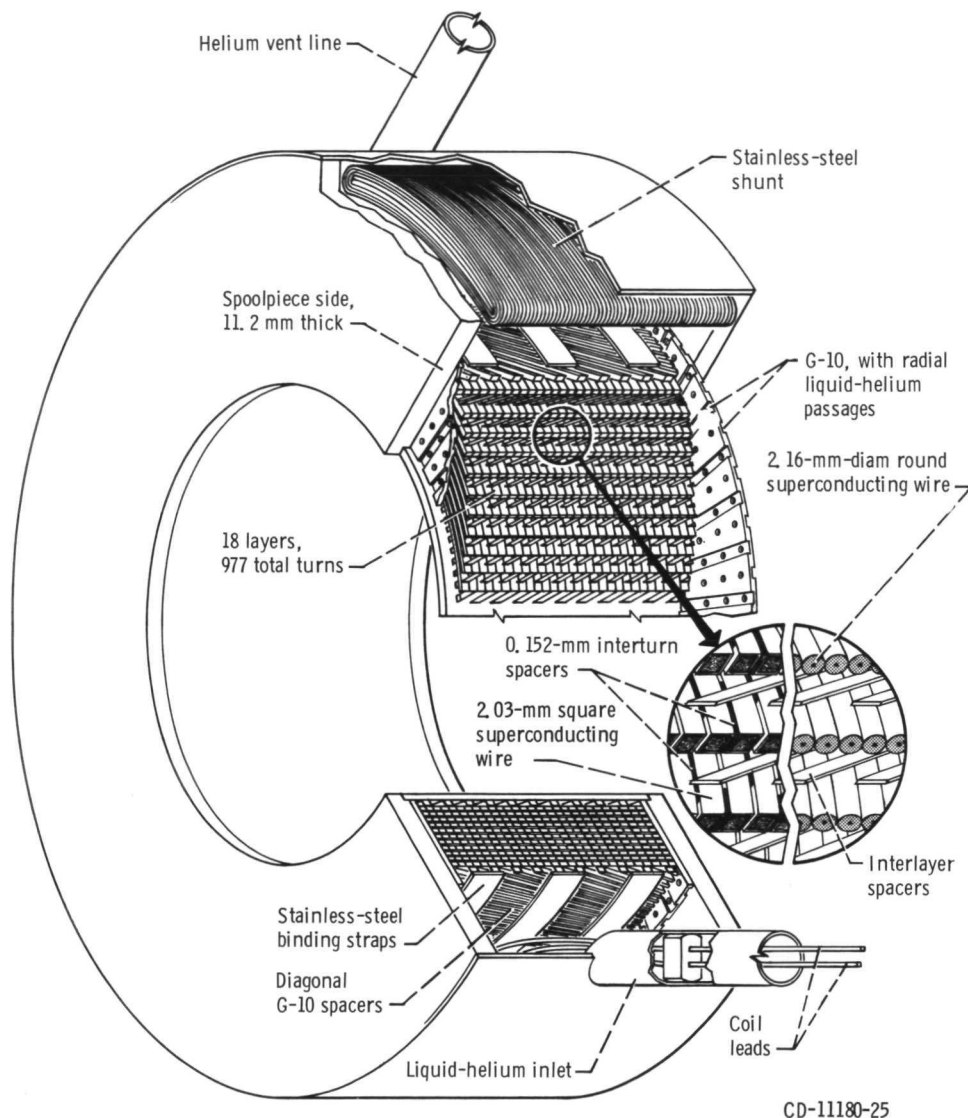


Figure 8. - Isometric cutaway drawing of one of the 12 superconducting coils. Winding details are not to scale in that the actual coils had 18 radial layers and approximately 54 turns along the axis per layer. Insert shows details of cooling passages utilized in both round and square wire coils. Inside diameter of spoolpiece, 210 millimeters; outside diameter of spoolpiece, 406 millimeters; inside diameter of windings, 218 millimeters; outside diameter of windings, 305 millimeters; axial width of windings, 120 millimeters; axial width of spoolpiece, 146 millimeters.

millimeters long and are spaced approximately 6.3 millimeters apart. The radial passageways formed by adjacent turns on a given layer allow liquid helium to penetrate the windings radially to irrigate the individual wires. Radial flow of liquid helium also occurs through radial slots in the G-10 glass epoxy material which insulates the windings from the spoolpieces. This material is alternately slotted on both sides, and holes are drilled through the slots to permit liquid helium to penetrate inner layers of the winding. The liquid helium also irrigates the upper and lower surfaces of a given layer of wire

through cooling passages formed by diagonal strips of 0.38-millimeter-thick G-10 material. Thick diagonal pieces of G-10 mounted at the inner and outer circumference of the windings also promote the flow of liquid helium throughout the coil volume. The arrangement of cooling passages in a square wire coil is illustrated in figure 9.

The insert in figure 8 shows in detail the cooling passage configuration of the round and square wire used for the coils. The stability properties of the round wire are such that radial cooling passages are not required to meet the design current. The round wire is therefore wound without any spacing between individual turns on each layer. The adjacent layers, however, are separated by diagonal G-10 material in the same manner as the square wire.

As indicated in figure 8, each of the 12 coils has a shunt in parallel with the coil, which serves to dissipate the stored magnetic energy in the event of a coil normalcy. Each shunt consists of a type 304 stainless-steel strip approximately 11.4 centimeters wide, 160 centimeters long, and 0.46 millimeter thick. The stainless-steel strips were

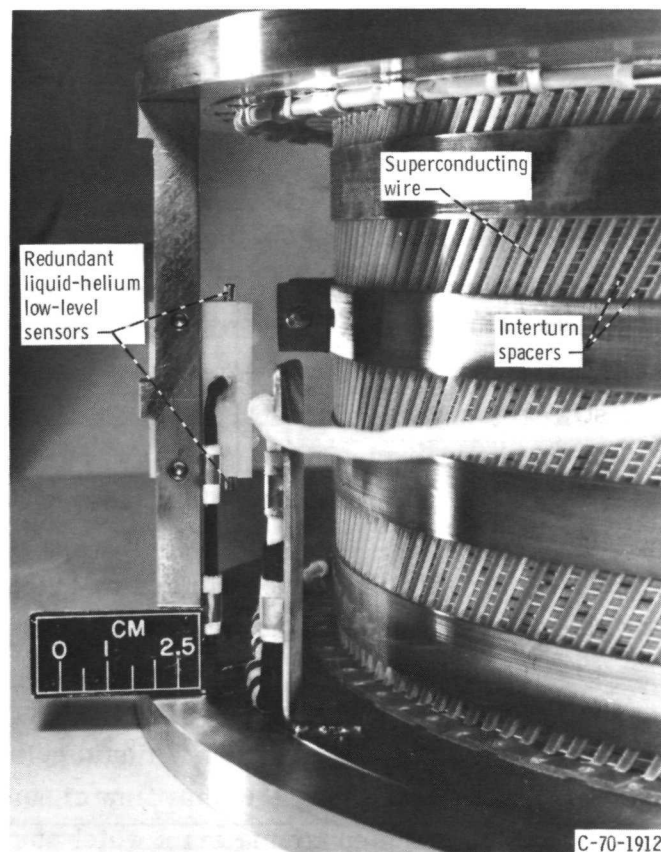


Figure 9. - Closeup of a coil.

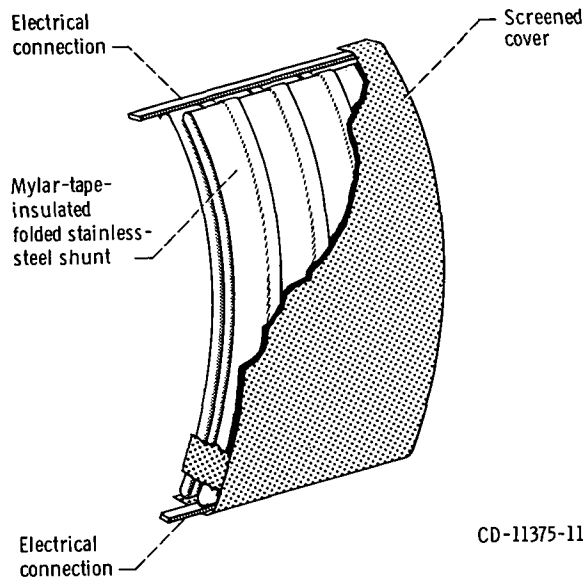
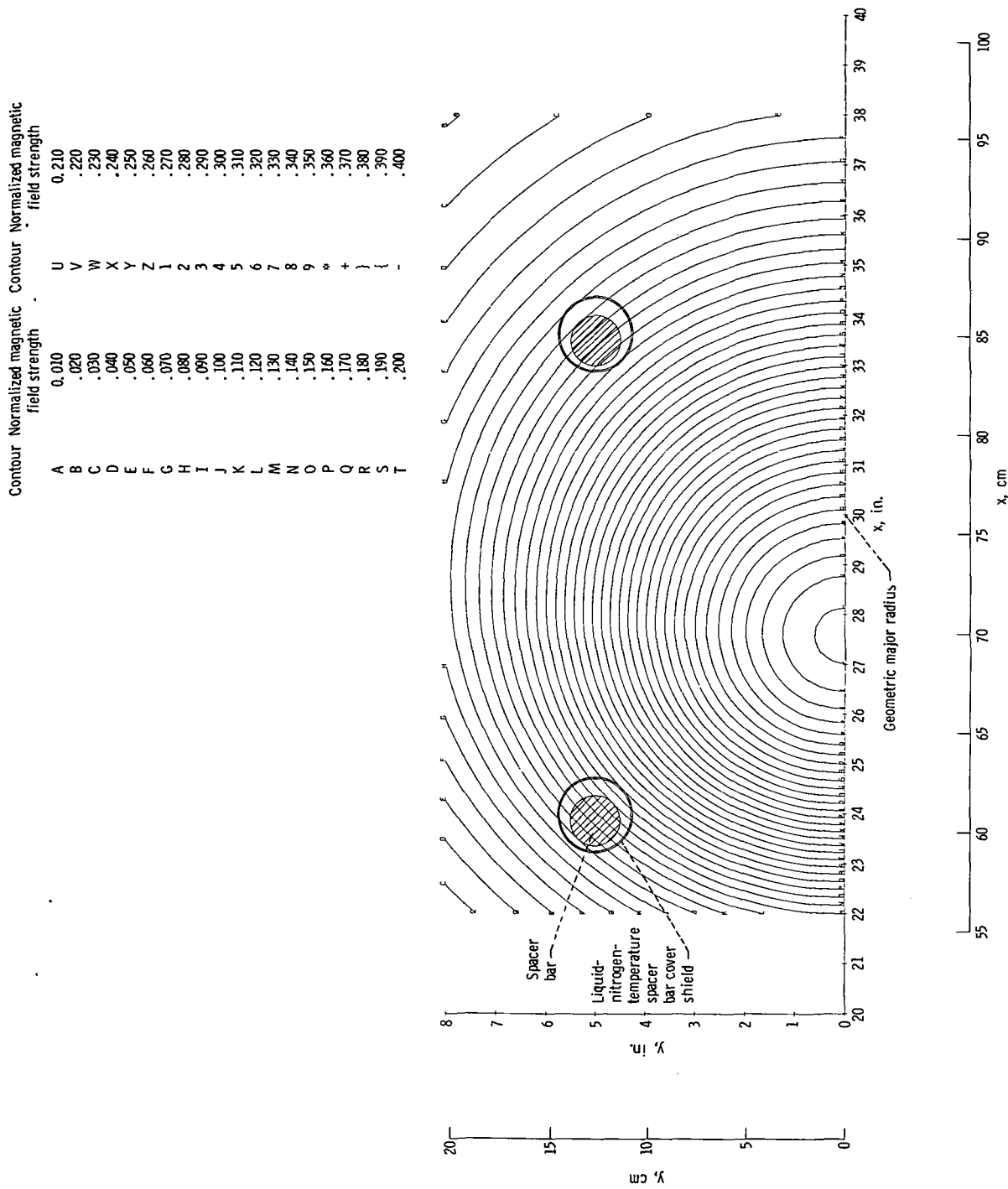


Figure 10. - Sketch of shunt construction. A stainless-steel strip was folded into a flat coil and fitted into magnet spoolpiece between the windings and coil canister.

insulated on both sides with Mylar tape and then rolled up and folded flat into the configuration shown at the top of figure 8. Figure 10 shows the details of the shunt construction.

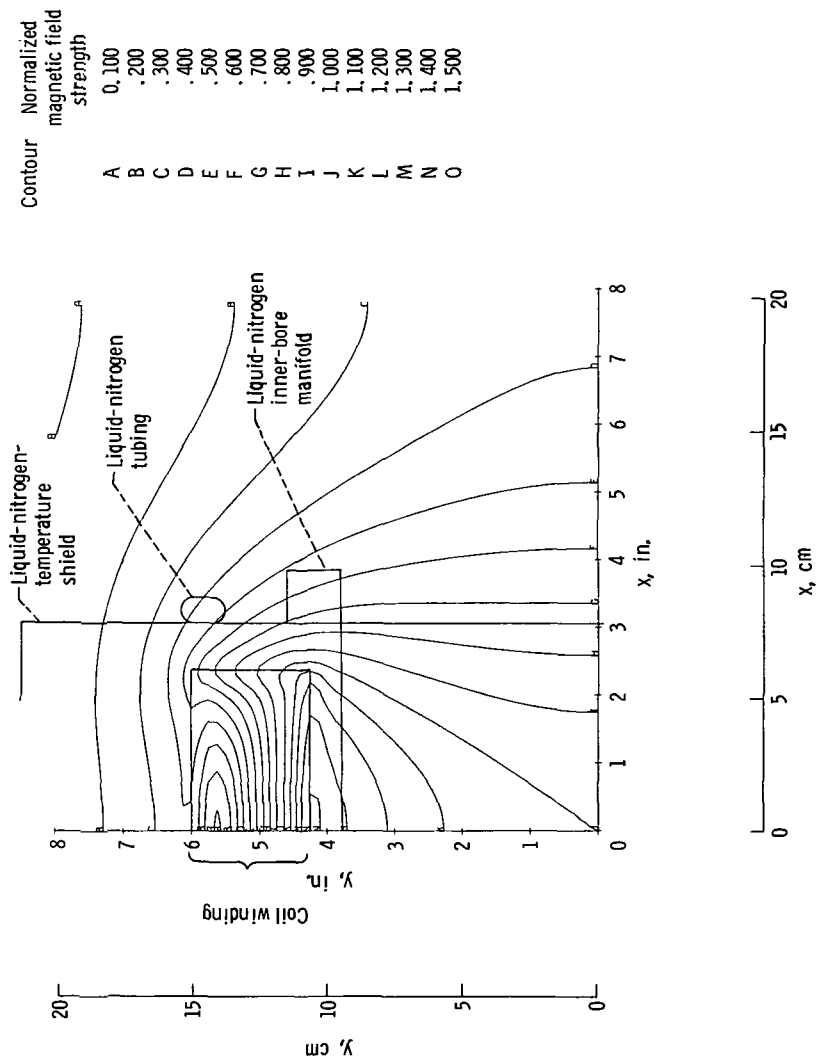
The total magnetic field resulting from the 12 coils, the properties and winding dimensions of which are shown in figure 8, was calculated by a computer program which summed the contribution of all 12 coils in the final assembly. In figure 11 are shown the contours of magnetic field strength in three planes. Figure 11(a) shows the magnetic field strength in a plane containing the toroidal axis and halfway between two of the coils. The approximately circular magnetic field strength contours have their center at the magnetic axis, which is displaced inward approximately 6.1 centimeters from the geometric axis of the system. Figure 11(b) shows an elevation along a cylindrical surface, the radius of which is the major radius of the torus. The field strength contours are shown from the plane of a coil to a midplane. Figure 11(c) shows a plan view of the magnetic field strength contours in the equatorial plane of the torus. The magnetic field strength is shown inside and outside the windings of one coil and in the volume of space occupied by the plasma. In the contour plots in figure 11, the sheet metal has been sketched in to indicate the volume of useful magnetic field available for plasma physics experimentation in this facility.

Figure 12 shows the distribution of magnetic field lines in this facility. Figure 12(a) is a plan view of the magnetic field lines in the same plane as figure 11(c). The magnetic



(a) Relative magnetic field strength contours in a plane containing toroidal major axis and halfway between two of the 12 superconducting coils.

Figure 11. - Contours of magnetic field strength calculated for entire 12-coil array. Relative magnetic field strength is plotted with value on axis at coil midplane normalized to unity.

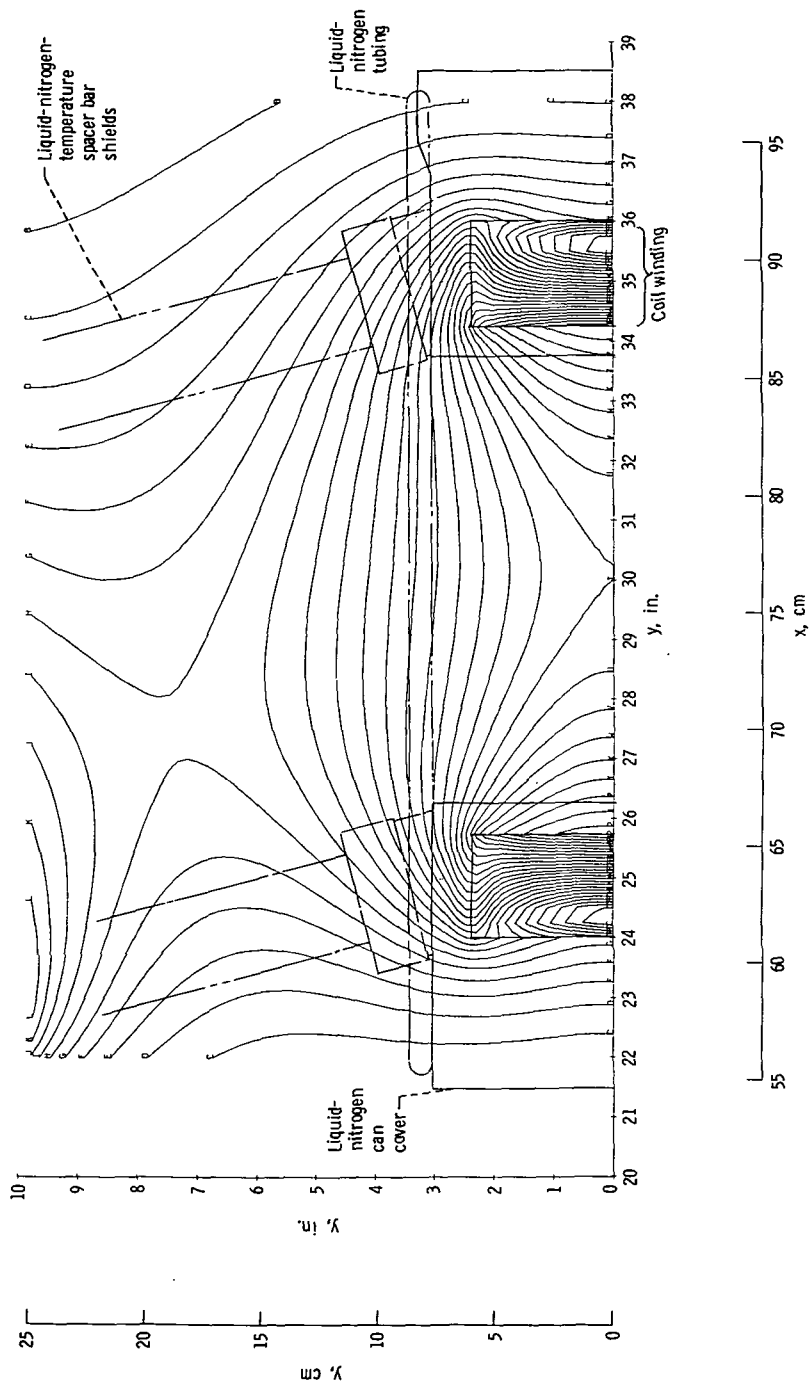


(b) Elevation of magnetic field strength along cylindrical surface the radius of which is equal to major radius of torus.

Figure 11. - Continued.

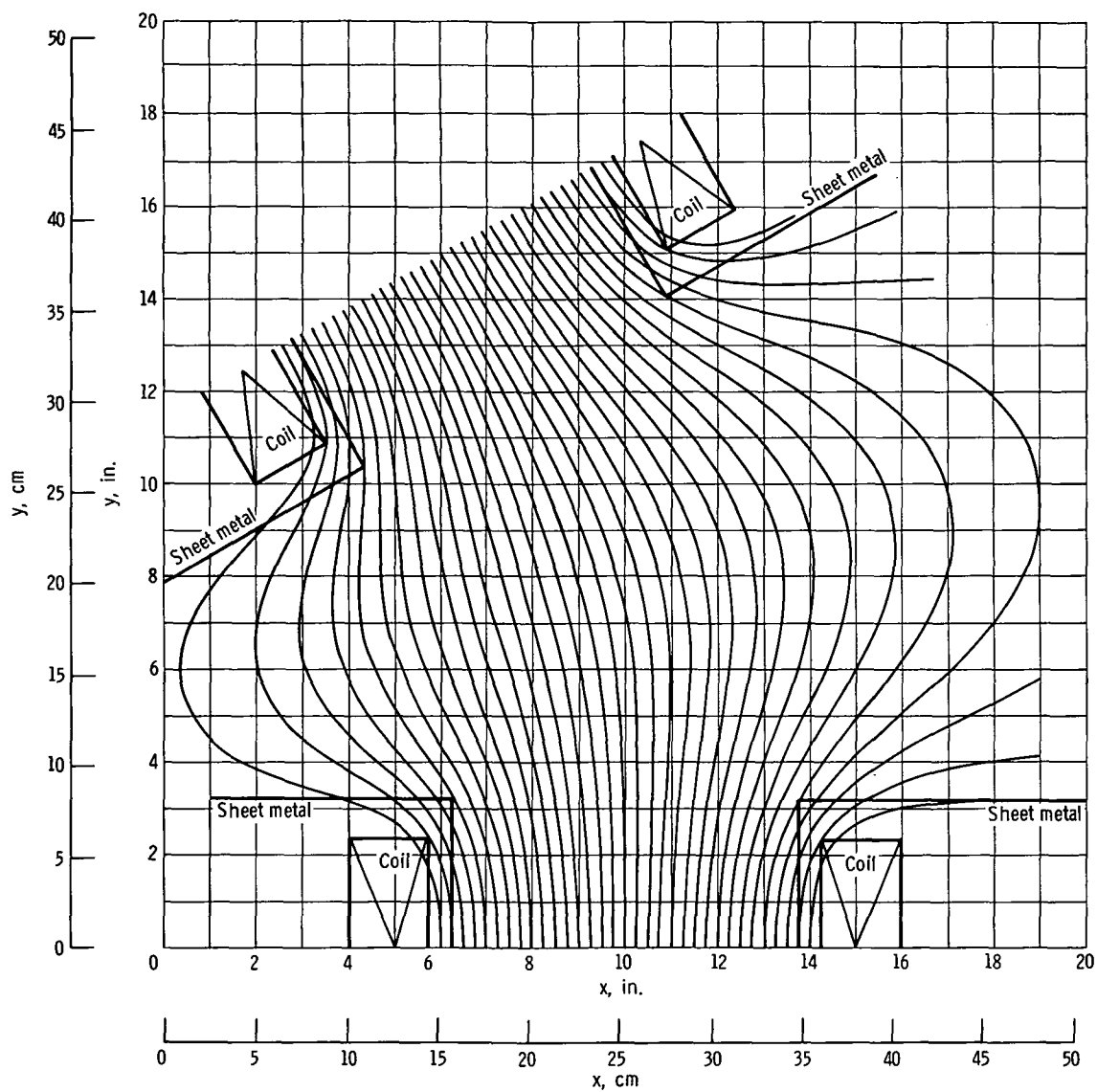
Contour Normalized magnetic field strength

A	0.050	Q	0.850
B	.100	R	.900
C	.150	S	.950
D	.200	T	1.000
E	.250	U	1.050
F	.300	V	1.100
G	.350	W	1.150
H	.400	X	1.200
I	.450	Y	1.250
J	.500	Z	1.300
K	.550	1	1.350
L	.600	2	1.400
M	.650	3	1.450
N	.700	4	1.500
O	.750	5	1.550
P	.800	6	1.600



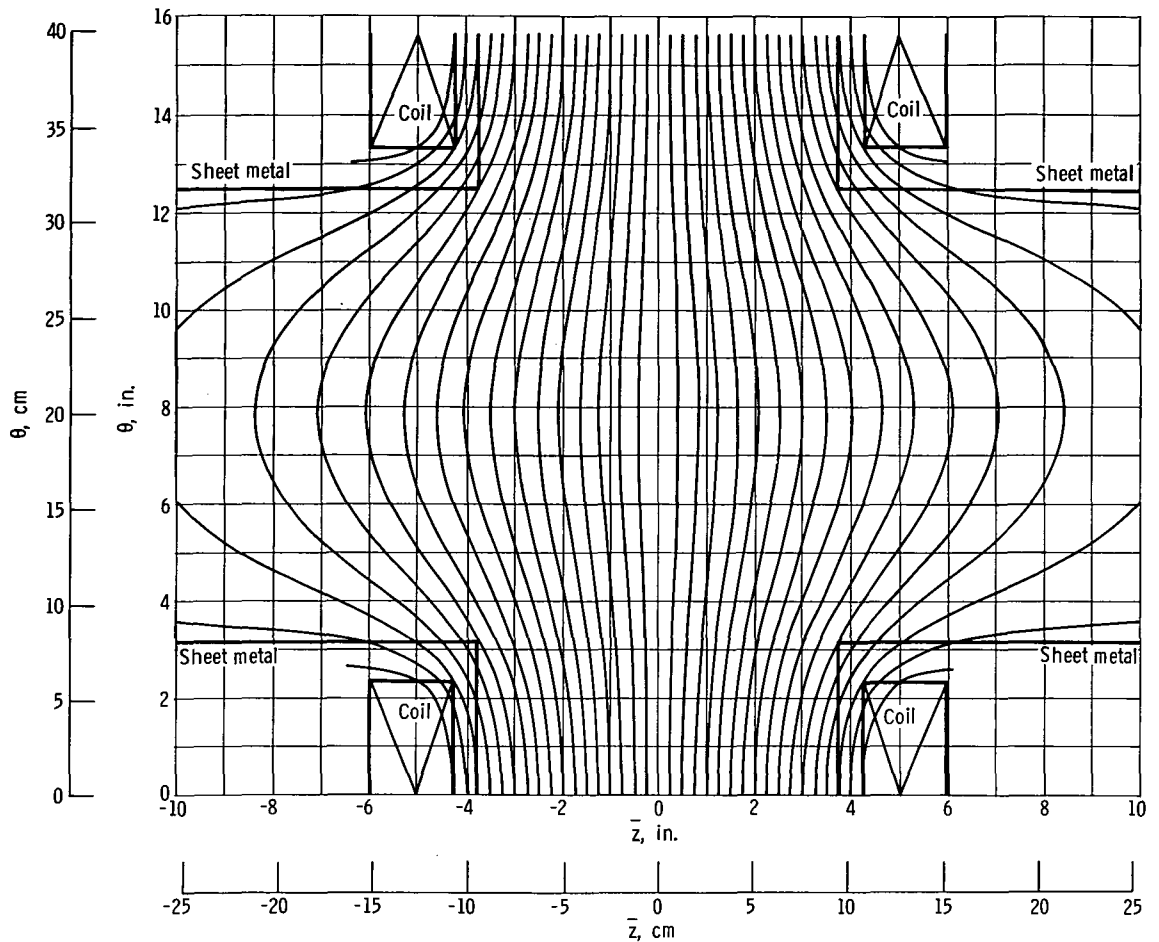
(c) Plan view of magnetic field strength in plane of torus, from center of one of the 12 coils to the midplane.

Figure 11. - Concluded.



(a) Magnetic field line distribution in equatorial plane of torus.

Figure 12. - Magnetic field line distribution between two coils as result of magnetic field of all 12 coils.



(b) Magnetic field line distribution on cylindrical surface equal to major radius of torus.

Figure 12. - Concluded.

field lines neck down in the region of maximum field strength under the coils and bow out in the regions between adjacent coils. The plasma follows these magnetic field lines in the manner illustrated in figure 2. Figure 12(b), like figure 11(b), is an elevation of the magnetic field line distribution in a cylindrical surface, the radius of which is the major radius of the torus.

Each superconducting coil was wound on a spoolpiece, the dimensions of which are given in figure 8. This spoolpiece consists of two side pieces welded to an inner cylinder 21 centimeters in inside diameter. The sides of the spoolpiece are approximately 11.2 millimeters thick and consist of type 304 stainless steel. There is a circumferential volume with a radial thickness of 5.1 centimeters between the outer circumference of the superconducting windings and the outer circumferential shell of the liquid-helium canister. This volume is used to house the shunt, the liquid-level sensors, and the liquid helium. This outer can is welded circumferentially to the edges of the spoolpieces.

Mechanical Design

The magnetic forces acting between adjacent coils were borne by four spacer bars; an exploded view of one spacer bar is shown in figure 13. It was necessary to fabricate the spacer bars in three pieces in order to assemble them after the coils were mounted in place. At one end of each spacer bar is a turnbuckle assembly which permits adjustments in the spacing between adjacent coils.

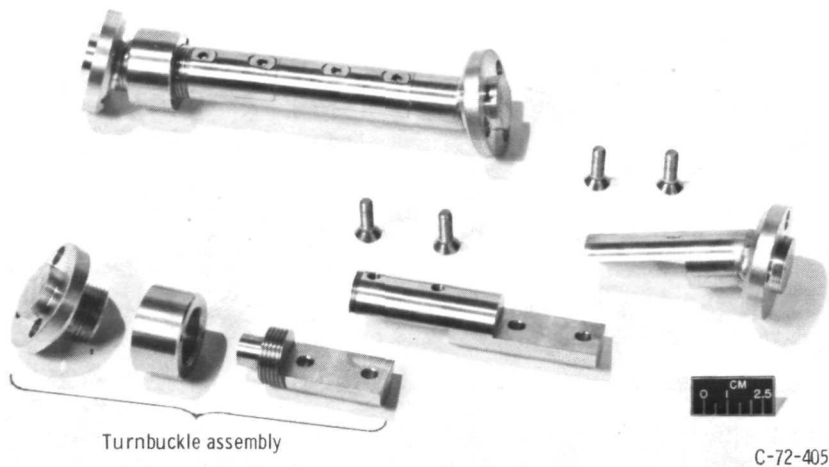


Figure 13. - Spacer bar used to support compressive forces between individual coils. A spacer bar like that shown was located on inner side of each coil pair. The threaded nut at one end of the spacer bar is a turnbuckle arrangement for adjustment of spacing between coils.

Figure 14 depicts three coils in various stages of fabrication. On the right side is a coil without its outer can welded in place. The center coil has the liquid-helium can cover welded in place, and the left coil has the liquid-nitrogen temperature shield mounted around the liquid-helium temperature canister. Between the coils are the spacer bars, several of which are covered by heat shields. Also evident in figure 14 is the manner in which the coils are mounted to the upper helium manifold. This stainless-steel manifold tube is 6.3 centimeters in minor diameter, with a wall thickness of 5.1 millimeters. The weight of the 12 coils is borne by tabs which are welded to the upper liquid-helium manifold. This manifold is suspended from six yokes which are attached to the liquid-helium reservoirs.

Figure 15 includes one of the liquid-helium reservoirs above the coil assembly. A liquid-nitrogen temperature shield surrounds the reservoir tank. There are three such reservoirs, each one of which has a capacity of 0.1 cubic meter (100 liters) of liquid helium. The entire coil assembly and the upper liquid-helium manifold is suspended from two yokes at either end of each of the three reservoir tanks. The weight is trans-

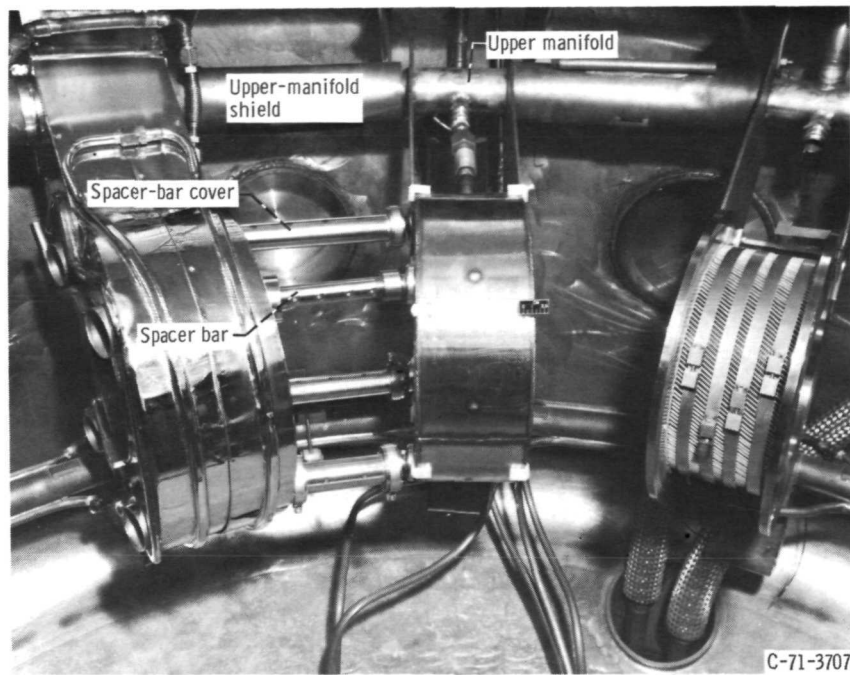


Figure 14. - Three coils in various stages of assembly mounted on the upper liquid-helium manifold.

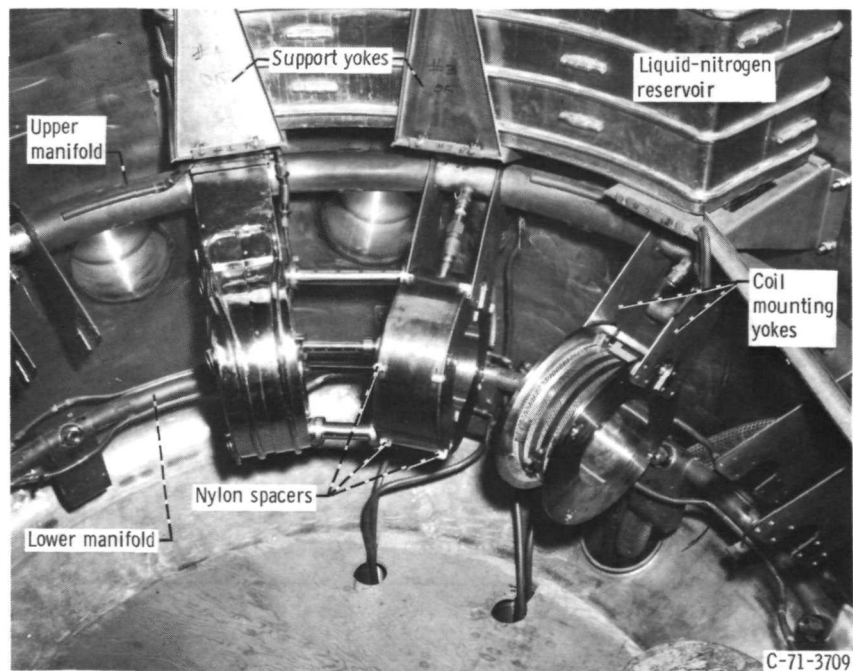


Figure 15. - Three coils mounted in system, with liquid-helium reservoir showing above them.

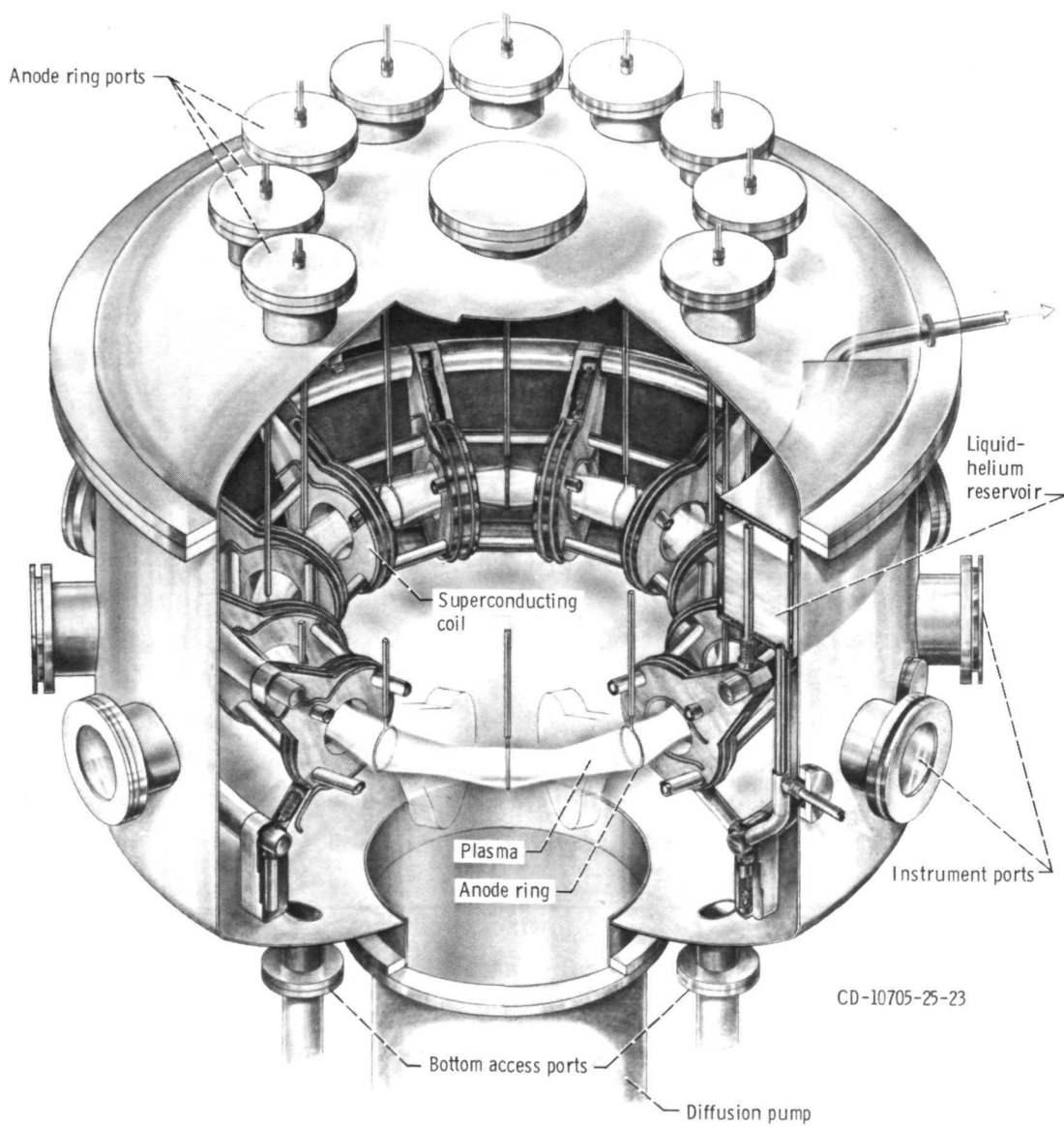


Figure 16. - Isometric cutaway view of entire magnet facility.

mitted from the upper liquid-helium manifold to the bottom of the liquid-helium reservoir tank. This load is then transmitted to the upper portion of the reservoirs, which are suspended from a structure at liquid-nitrogen temperature by a yoke assembly which surrounds the liquid-nitrogen canister of the reservoir. The weight of the magnet facility is supported by nine brackets, three at the bottom of each liquid-helium reservoir.

Figure 16 is an isometric cutaway drawing of the entire magnet facility. The 12 superconducting coils and the three reservoirs equally spaced in the vacuum tank above them are shown. Figure 16 illustrates the 12 anode rings located midway between the 12 coils and the approximate locations of the plasma created in this facility.

The venting helium gas rises through the upper connection to the coil canisters, through the upper liquid-helium vent manifold, and through a standpipe to the top of the three liquid-helium reservoirs. The vented gas travels along the top of the reservoirs and out liquid-helium vent lines located at two stations in the vacuum tank. One of the liquid-helium vent lines contains the coil power leads and the coil sensor leads, which are cooled by the venting helium gas.

Cryogenic System Design

On the basis of operational experience with the pilot rig, it was expected that each of the 12 coils would boil off approximately 75×10^{-5} cubic meter (0.75 liter) of liquid helium per hour in the steady state. The bumpy-torus facility had additional heat loads associated with the three liquid-helium reservoirs, for which there was no equivalent in the pilot rig. There was also a significant heat leak through the copper bus bars which were required to carry as much as 700 amperes to the coils. The liquid-helium vent lines, sized to limit backpressure, introduce an additional heat leak.

A schematic of the liquid-helium flow system is shown in figure 17. The 12 superconducting coils are connected hydraulically in parallel across the upper and lower liquid-helium manifolds. There are three distinct modes of operation for the liquid-helium system, cooldown, running, and replenishment. The first is a cooldown of the entire liquid-helium system from room temperature. This is accomplished in part by a "cold soak," in which liquid nitrogen is caused to flow through the liquid-nitrogen shields. After the liquid-helium system approaches liquid-nitrogen temperature, the three bypass valves which lead from the lower manifold directly to the three liquid-helium reservoir tanks are closed. The main liquid-helium valve is opened and this forces the liquid helium to flow through the coils, to the upper manifold, and from the upper manifold into the reservoirs. This mode of cooling is used until the coils are filled with liquid helium. At this point, the three bypass valves to the reservoirs are opened, and the reservoirs are filled with liquid helium without its being forced through the manifolds and the 12 coils.

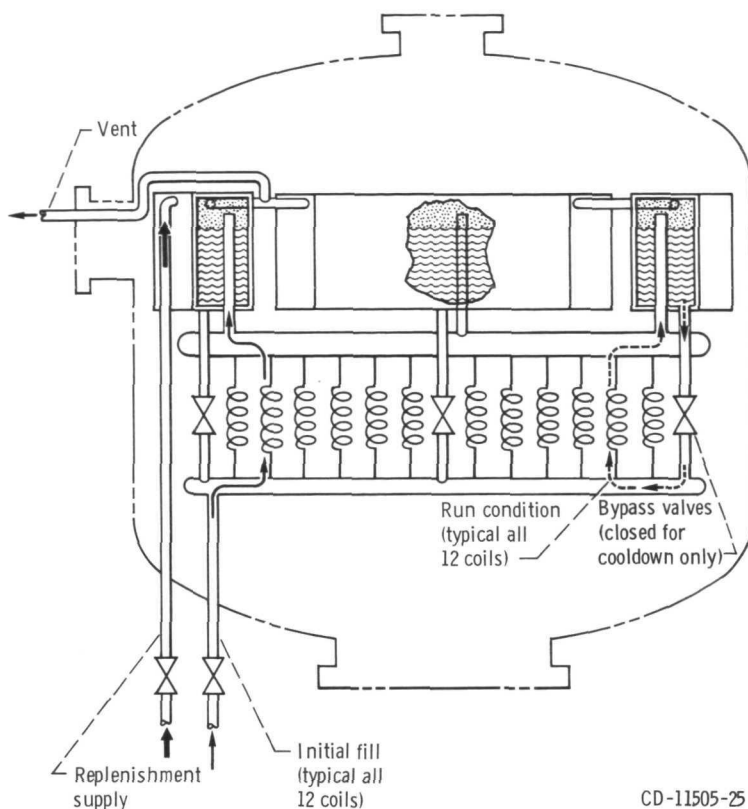


Figure 17. - Schematic drawing of liquid-helium flow system. The two modes of operation indicated are for initial filling with liquid helium and for filling while magnets are fully charged.

The liquid helium is transferred from the storage Dewar to the facility by a commercially manufactured liquid-helium transfer line. This transfer line has a tee with two valves immediately outside the vacuum tank. One valve is opened to permit liquid helium to flow through the manifolds and coils to the reservoir during cooldown, and the replenishment valve is opened when it is desired to allow the liquid helium to flow directly into the upper reservoir tanks.

While running, the lower manifold is connected directly to the liquid-helium reservoirs. Liquid helium circulates from the reservoirs into the lower liquid-helium manifold and then into the bottom of the 12 coils. The vent gases produced in the coils percolate through the upper liquid-helium vent line to the upper liquid-helium manifold. The vent gases then travel to the three reservoir tanks through a standpipe in each of the liquid-helium reservoirs.

An unusual feature of this facility is the extensive use of 2.54-centimeter (1-in.) AN fittings. All joints at liquid-helium temperature which utilized AN fittings contained either sensor cable or magnet leads. Altogether this magnet facility contains 36 AN fit-

tings at liquid-helium temperatures, and it also contains 24 stainless-steel bellows between the coils and the upper and lower liquid-helium manifolds. Figure 18 shows a 2.54-centimeter (1-in.) AN fitting which was used successfully in a coil pair test. This is a standard stainless-steel-to-stainless-steel AN connection. Special precautions must be taken to prevent leaks from developing when such AN fittings are used at liquid-helium temperatures and in a vacuum environment. These precautions included covering the mating surfaces with Teflon tape and torquing the fittings to a least 135 newton-

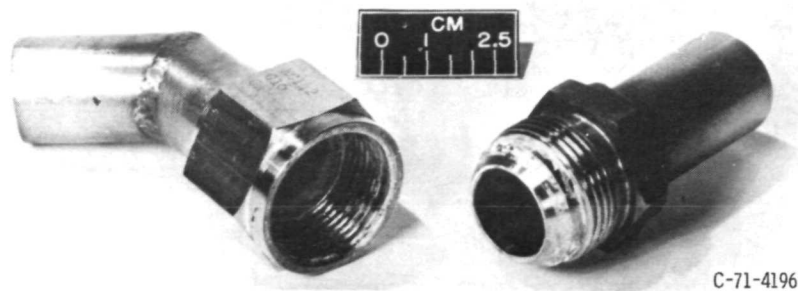
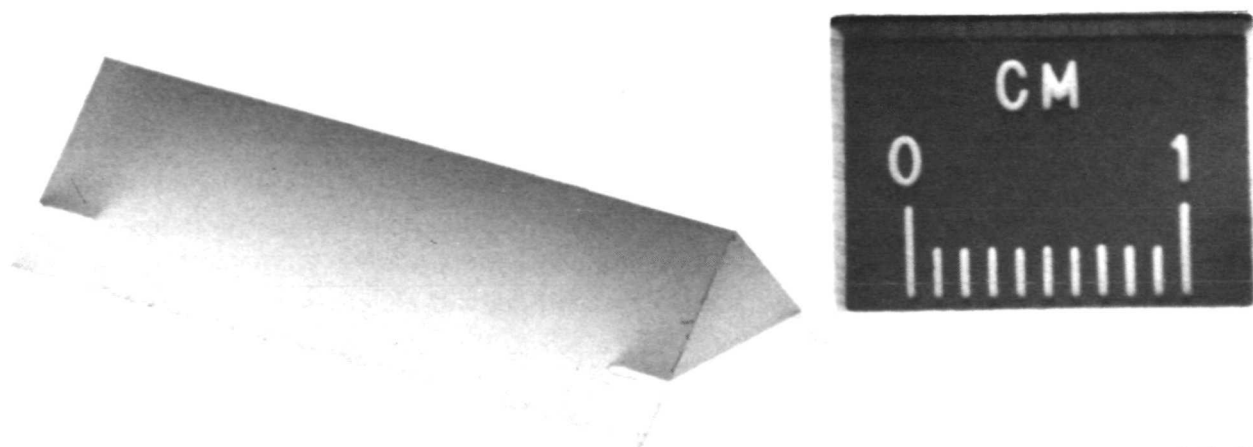


Figure 18. - Army-Navy (AN) fitting 2.54 centimeters (1 in.) in diameter, taken from the coil pair test apparatus.

meters (100 ft-lb) in order to assure a leak-tight connection. In addition to these precautions, it was necessary that a high standard of workmanship be employed in joining the AN fittings and assuring that the mating surfaces were not burred or scratched.

In this facility, a positive means of holding spacers to the liquid-helium surfaces was adopted; it is illustrated in figure 19. This shows a typical triangular nylon spacer. The base of the triangle is flat on the liquid-helium-temperature surface, and the apex of the triangle is in contact with the liquid-nitrogen canister. The spacer is attached to the liquid-helium surface by two thin stainless-steel straps which are spot welded to the liquid-helium canister. The stainless-steel straps fit two slots cut in the ends of the triangular prism which forms the spacer. These proved quite satisfactory in serving their intended function. The placement of the nylon spacers on the liquid-helium canisters is visible in figures 14 and 15.

Figure 20 is a schematic drawing of the liquid-nitrogen flow system, which is fed from a central Dewar. The liquid nitrogen flows continuously, and the venting material contains both liquid- and vapor-phase nitrogen. The liquid nitrogen in the venting gases is recovered and recirculated. The liquid-nitrogen flow system in this facility consists of seven separate and parallel flow paths. Two of these liquid-nitrogen circuits each cool the inner bores of six liquid-nitrogen can covers. These circuits are intended to carry away the radiant heat loading from the plasma which is deposited on the inner bore



C-72-1883

Figure 19. - Triangular nylon spacer used to prevent thermal contact of liquid-nitrogen and liquid-helium systems.

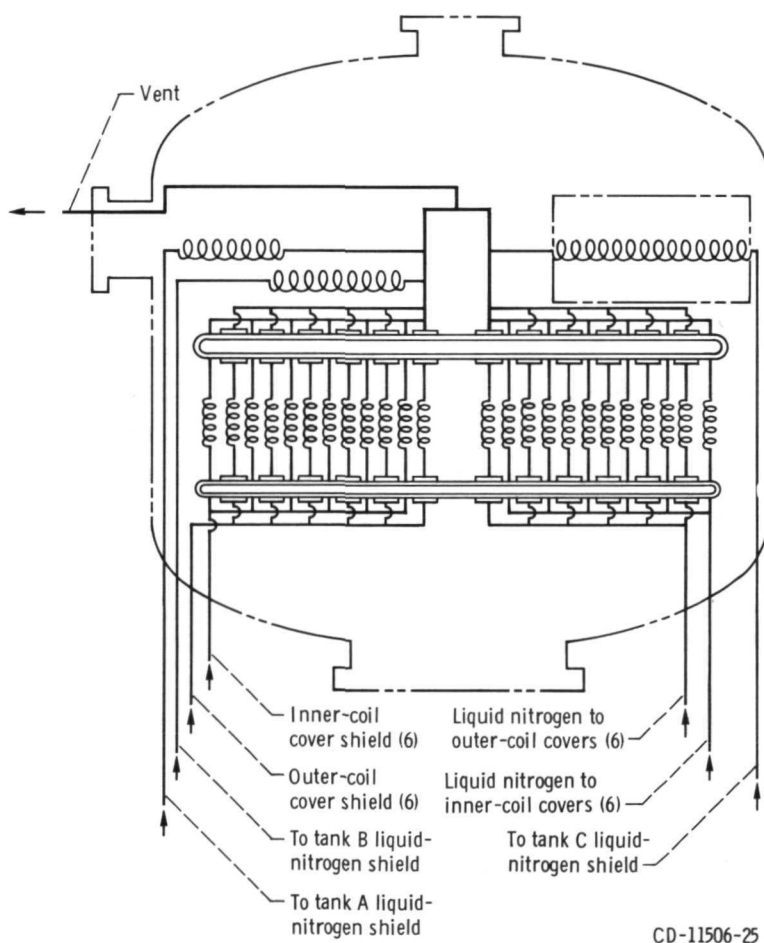


Figure 20. - Schematic drawing of liquid-nitrogen flow system.

of the coil assemblies. There are, in addition, two liquid-nitrogen circuits, each including six coils, which snake around the remainder of the liquid-nitrogen can covers and remove the radiant heat loading on them. Three liquid-nitrogen circuits cool the outer liquid-nitrogen jackets around the three liquid-helium reservoir tanks. These seven liquid-nitrogen circuits coalesce in a single liquid-nitrogen vent manifold, which is connected to the building recovery line.

Figure 21 is an isometric view of a liquid-nitrogen can cover showing the inner bore cooling. The inner bore is closest to the plasma and receives the largest flux of radiant heat energy. The liquid nitrogen is forced to flow through a system of zigzagged axial passages from an inlet manifold to an outlet manifold 180° away. This design was intended to minimize the amount of radial space taken by the cooling passages, while at the same time permitting the removal of a substantial loading of radiant energy. The liquid-nitrogen can cover is made of copper and chrome plated to minimize the amount of absorbed gases and dirt acquired during the fabrication and assembly process. The remainder of the liquid-nitrogen heat shields are cooled by 0.95-centimeter (3/8-in.) copper tubing which is welded to the sheet metal base. This tubing is snaked over the surface in such a way as to cool the entire surface.

The upper and lower liquid-helium manifolds are covered by copper shields onto which are brazed liquid-nitrogen tubing. This tubing also serves as a parallel connection of the coils to the inlet and outlet liquid-nitrogen lines. In the liquid-nitrogen system, the six coils in each liquid-nitrogen jacket and inner-bore cooling assembly are hydraulically in parallel. Each of the four lines connecting the two liquid-nitrogen circuits to their manifolds contain a stainless-steel bellows to permit final fitting of each individual coil cover in position.

In the pilot rig, it was found that AN fittings could be used for liquid-nitrogen service in a vacuum system if copper tubing is mated to a stainless-steel fitting and the mating surfaces are covered with Teflon tape. There are approximately ninety-six 0.95- or 1.27-centimeter (3/8- or 1/2-in.) AN fittings in the liquid-nitrogen lines. There are approximately 420 silver-soldered connections in the entirety of the liquid-nitrogen flow system. The liquid-nitrogen shields surrounding the 12 coils, and the liquid-nitrogen shields surrounding the liquid-helium reservoirs above them, present approximately 18 square meters of liquid-nitrogen-temperature surfaces to the vacuum tank and provide a substantial cryopumping of impurity gases such as carbon dioxide (CO_2), water vapor, and any pump oil that might otherwise be present to contaminate the experiment. It was intended that the liquid-nitrogen flow through each of the 12 coils be adequate to remove 2 kilowatts of radiant energy from the liquid-nitrogen can covers, thus yielding a total heat-removal capability of 24 kilowatts from the liquid-nitrogen can cover assemblies.

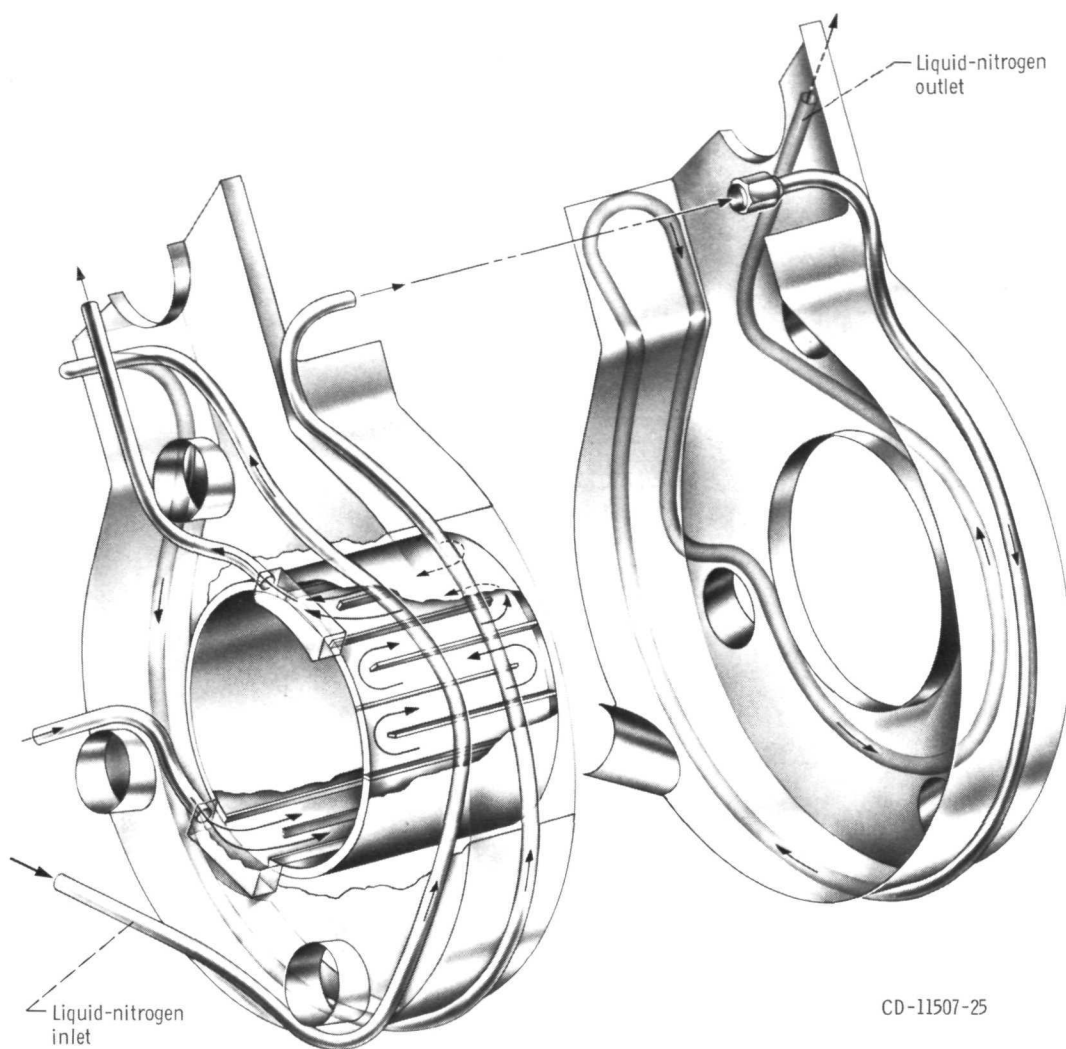


Figure 21. - Isometric view of liquid-nitrogen can cover, showing provision for cooling inner bore of cover.

Vacuum System Design

A schematic of the vacuum system employed in this facility is shown in figure 22. The vacuum tank itself is evacuated by a 0.141 cubic-meter-per-second (300 CFM or 141 liter/sec) mechanical forepump which is connected to a 81-centimeter (32-in.) diffusion pump with a rated pumping speed of 32 cubic meters per second (32 000 liters/sec). The diffusion pump is filled with silicone 705 oil and is fitted with a water-cooled end cap on the diffusion column. Between the diffusion pump and the vacuum tank is a liquid-nitrogen cold baffle to prevent backstreaming of the diffusion pump oil into the vacuum tank. Between the vacuum tank volume and the liquid-nitrogen baffle is a pumping speed controller, which permits independent variation of the background pressure and pumping

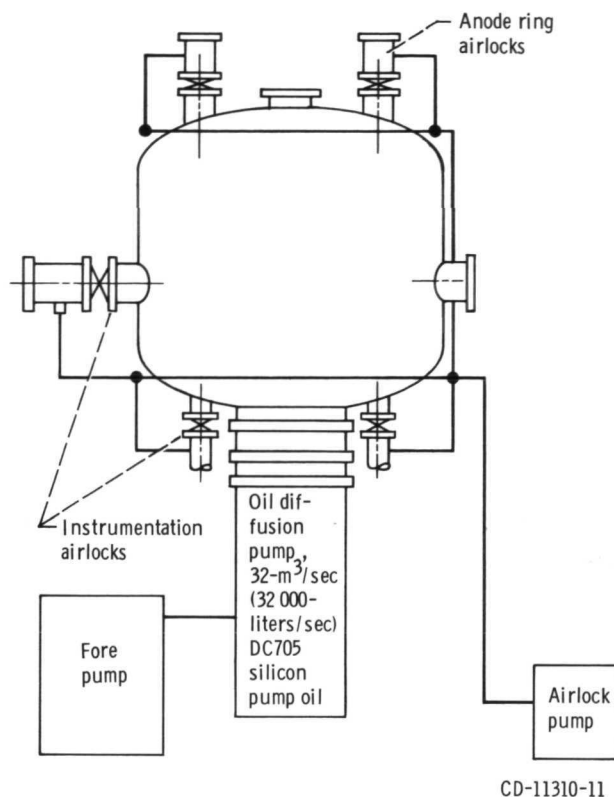
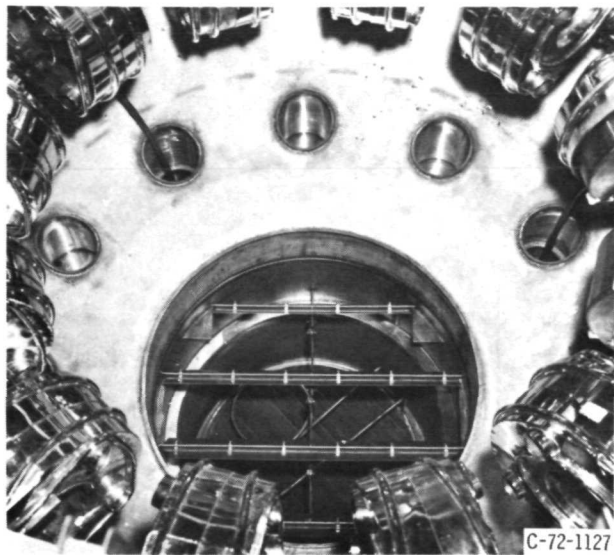


Figure 22. - Schematic of vacuum system, including auxiliary pumps.

speed of the pumping system. It is anticipated that the principal operating gas will be hydrogen or deuterium. Low background pressures or high throughput rates of gaseous hydrogen demand the full capacity of the diffusion pump. A high pumping speed is also desirable to handle the efflux of adsorbed gases from the liquid-nitrogen-temperature cryobaffles and heat shields as they warm up after a series of runs.

The pumping speed controller is shown in figure 23. Figure 23(a) shows the pumping speed controller with its flaps open, figure 23(b) shows the pumping speed controller with the flaps closed. These flaps are not intended to be vacuum tight but merely to provide a venetian-blind-like louvered control of the cross-sectional area of the pumping system.

The vacuum tank is constructed of type 304 stainless steel and is nonmagnetic. All fixtures and fittings of the magnet assembly are made of stainless steel or of nonmagnetic material to avoid perturbing the magnetic field in a way which might be detrimental to the experimental objectives. The vacuum tank is 2.59 meters in inside diameter and contains twelve 15.2-centimeter-diameter ports equally spaced around a 152-centimeter-diameter circle on the bottom of the vacuum tank. These ports are in the midplane of the plasma volume between each of the 12 magnetic field coils. Also providing access to the experimental volume are twelve 25.4-centimeter-diameter ports around the hor-



(a) Flaps open.



(b) Flaps closed.

Figure 23. - Pumping speed controller.

horizontal circumference of the vacuum tank. The axes of these twelve 25.4-centimeter-diameter ports are in the equatorial plane of the torus and permit visual and experimental access to the plasma volume. Two of the twelve 25.4-centimeter-diameter ports are canted at an angle to permit tangential access to the toroidal plasma ring in both clockwise and counterclockwise directions. The lid of the vacuum tank is removable and contains twelve 20.3-diameter ports through which the 12 anode rings are inserted. In addition to these 36 ports, there are six additional ports for the liquid-helium transfer line, for the liquid-nitrogen and liquid-helium vent, and for other service lines. Six of the twelve 15.2-centimeter-diameter bottom ports are utilized for liquid-nitrogen and other service lines.

Since it was anticipated that the facility would be kept at liquid-nitrogen temperatures for long periods of time, all 12 anode rings and all experimental diagnostic equipment are inserted into the tank through airlocks. Figure 24 shows an anode ring airlock assembly and the 20.3-centimeter-diameter gate valve required to close off the airlock assembly when the anode ring is retracted. Above the gate valve is the 20.3-centimeter-diameter airlock. On top of the airlock chamber is a brass flange with a ceramic fitting through which the 1.9-centimeter-diameter anode ring rod is inserted into the vacuum system. Figure 25 depicts one of the diagnostic airlocks on the side of the vacuum tank. The airlocks are evacuated by the auxiliary forepump shown in figure 22.

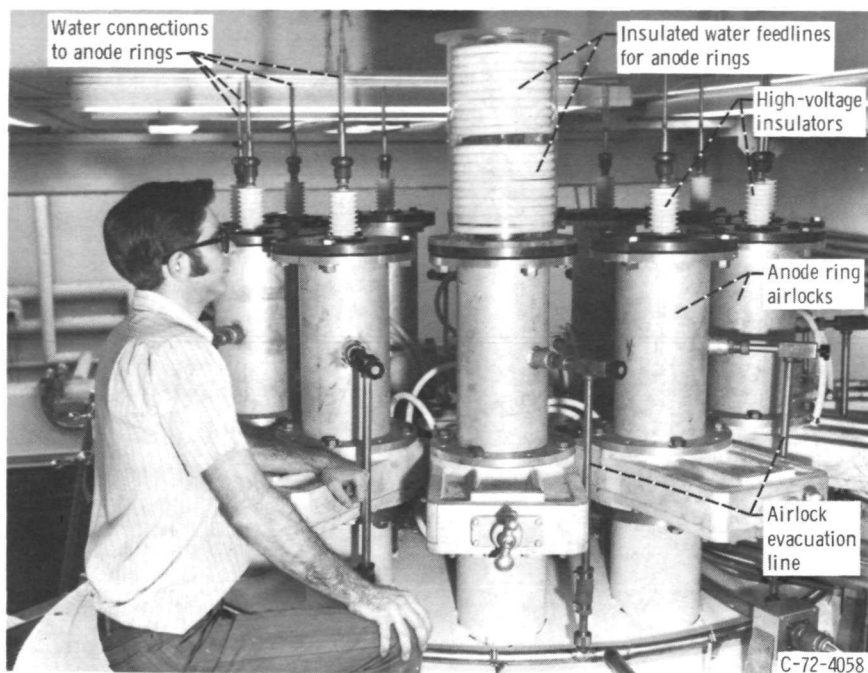


Figure 24. - Anode ring airlock assembly. Twelve of these were located on the twelve 20.3-centimeter (8-in.) diameter ports at top of vacuum tank shown in figure 16.

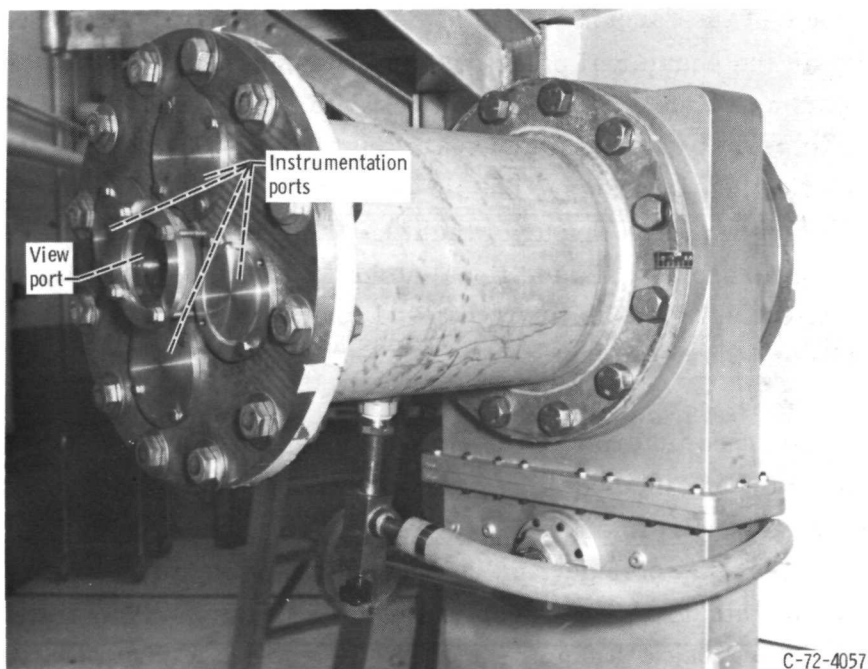


Figure 25. - Experimental airlock on one of the 25.4-centimeter-diameter side ports, through which diagnostic instrumentation is inserted into plasma.

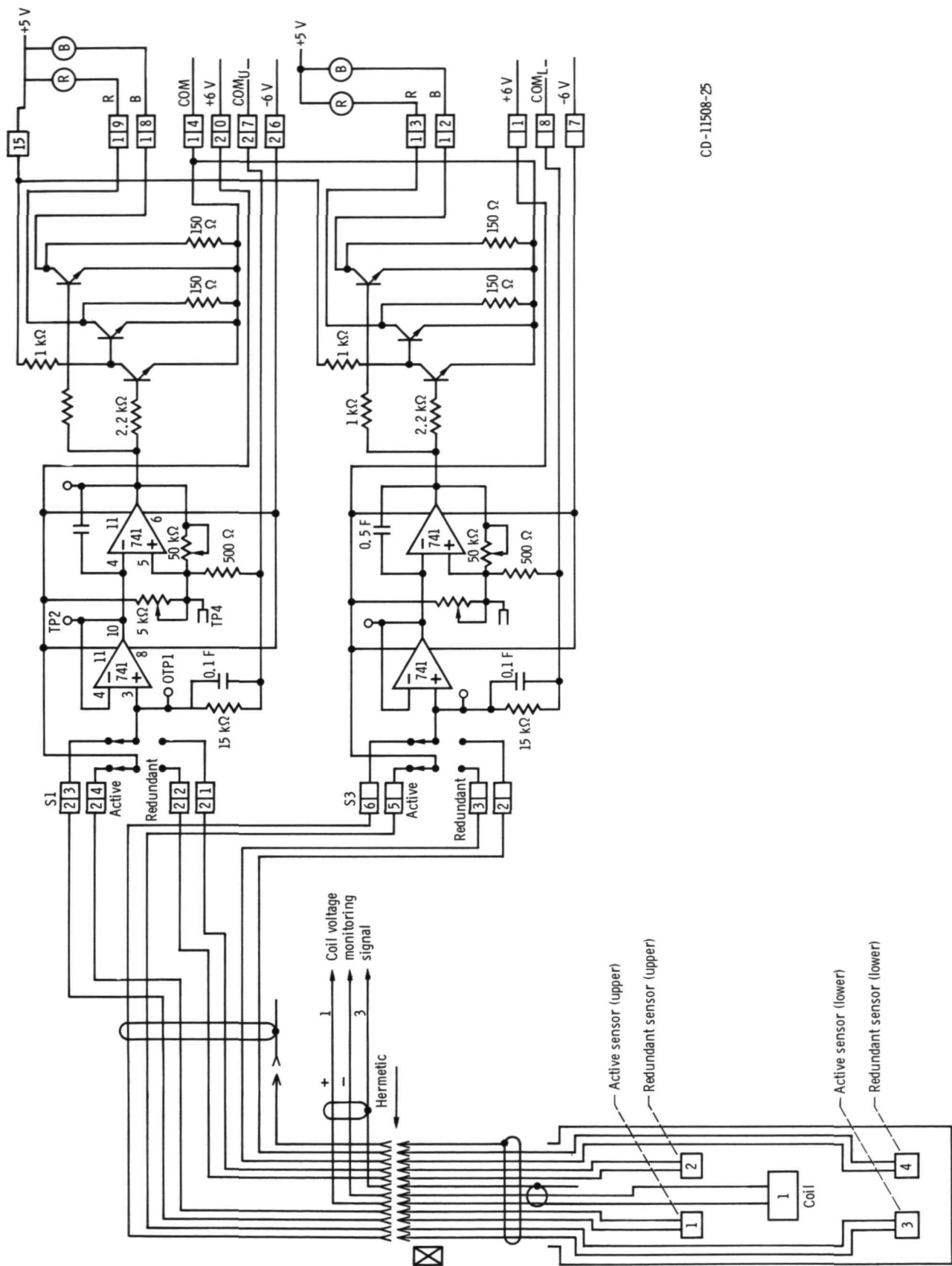
Instrumentation and Electrical Design

In a facility of this nature, it is essential to know the liquid-helium level in all components of the system which are supposed to be at liquid-helium temperatures and contain superconducting wire. Knowledge of the liquid-helium level is particularly important during early stages of facility testing before the acquisition of a body of experience to guide operating practice. Experience with carbon resistors on the pilot rig indicated that some other type of liquid-helium level sensor was essential on the present facility, and it also suggested that a redundant sensor be provided at each location.

Figure 26 is a diagram of the cryogenic instrumentation of a coil on this facility. Liquid-helium level sensors were installed at the bottom and top of the liquid-helium cans of all 12 coils. The bottom-most sensor indicates when liquid helium is starting to accumulate in the system. The high-level sensor in each of the 12 coils indicates if a vapor lock or other difficulty exists in any particular coil and also serves to warn when the liquid-helium level is dangerously low. In addition to these sensors, there are eight liquid-level sensors at equally spaced intervals in the three liquid-helium reservoir tanks. Altogether there are liquid-helium level sensors in 48 different locations throughout the system. Each one of these 48 positions has had a redundant spare sensor.

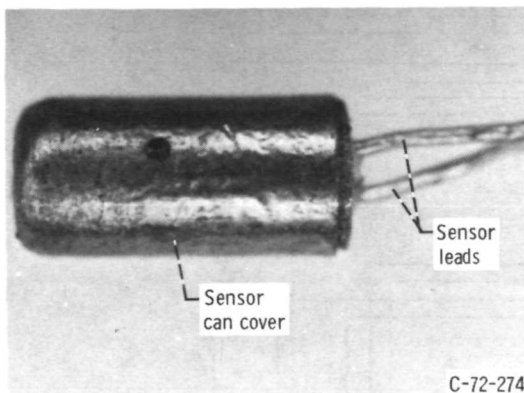
The liquid-level sensors used are shown in figure 27. Figure 27(a) is a closeup view of a single liquid-level sensor. This sensor is 2 millimeters in diameter and 5 millimeters along its axis. There are five holes in the cover through which the germanium sensing element contacts the liquid helium. Figure 27(b) is a closeup view of a liquid-helium-level sensor assembly. One of these is mounted at the bottom, the other at the top of the coil volume. The liquid-level sensor assembly consists of two sensors, one of which is redundant. The sensor assembly mounted on a coil is shown in figure 9. Figure 28 depicts the liquid-level sensor assembly used in the three liquid-helium reservoirs. Figure 28(a) shows the sensor boards apart, and figure 28(b) shows the sensor assembly together in the configuration in which it is mounted in the liquid-helium reservoirs. The individual sensors are mounted on printed circuit boards at intervals of 4 centimeters and are equally spaced from the bottom to the top of the liquid-helium reservoir. Figure 29 is a circuit diagram of one of the liquid-helium sensor circuits. This solid-state circuit is repeated for each one of the 48 active sensors used in the facility.

The electrical connections to the coils are illustrated in figure 30, which is a block diagram of the coil connections and the power supply. The 12 coils are hooked up in series, with only two leads connecting the coils to the power supply outside the liquid-helium environment. The voltage drop across each of the 12 coils is monitored by sensor leads attached to each coil. These voltage taps include the shunts as well as the coil windings and serve to indicate anomalous behavior of the coils and whether the coils are in the superconducting state.

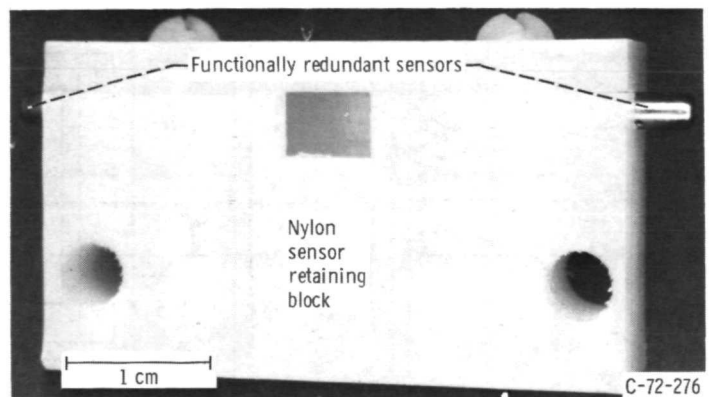


CD-11508-25

Figure 26. - Diagram of cryogenic instrumentation in bumpy-torus facility.

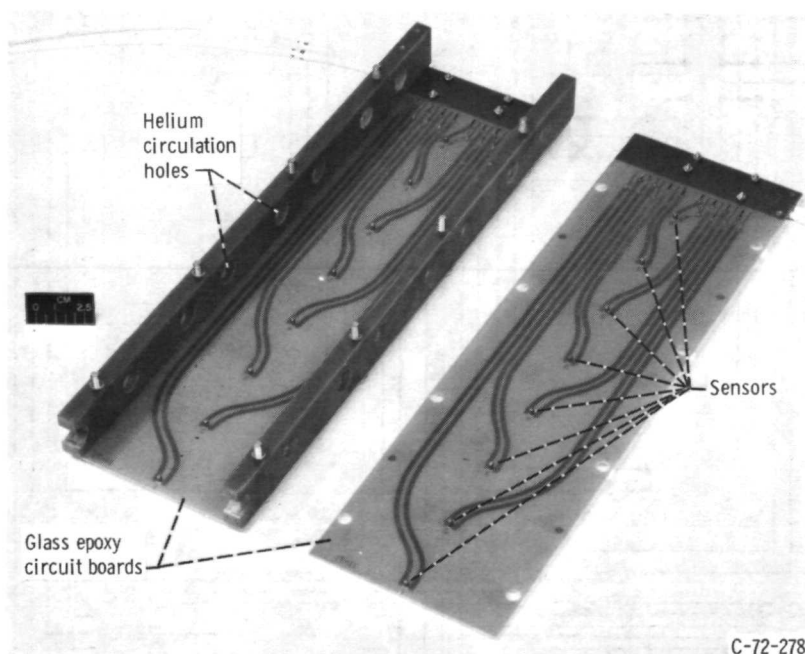


(a) Closeup of individual sensor.

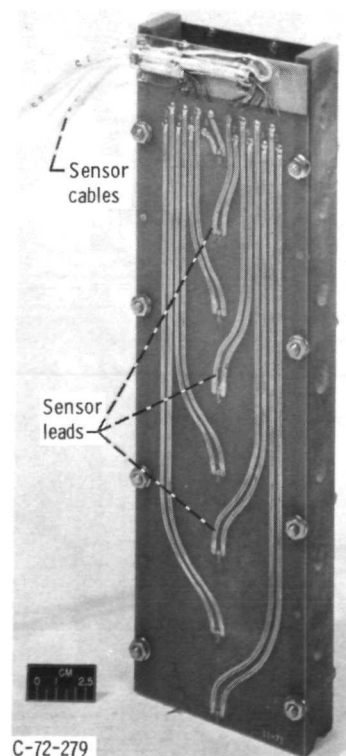


(b) Closeup of liquid-level sensor assembly, including the redundant sensor.

Figure 27. - Germanium liquid-level sensors used in the liquid-helium system.

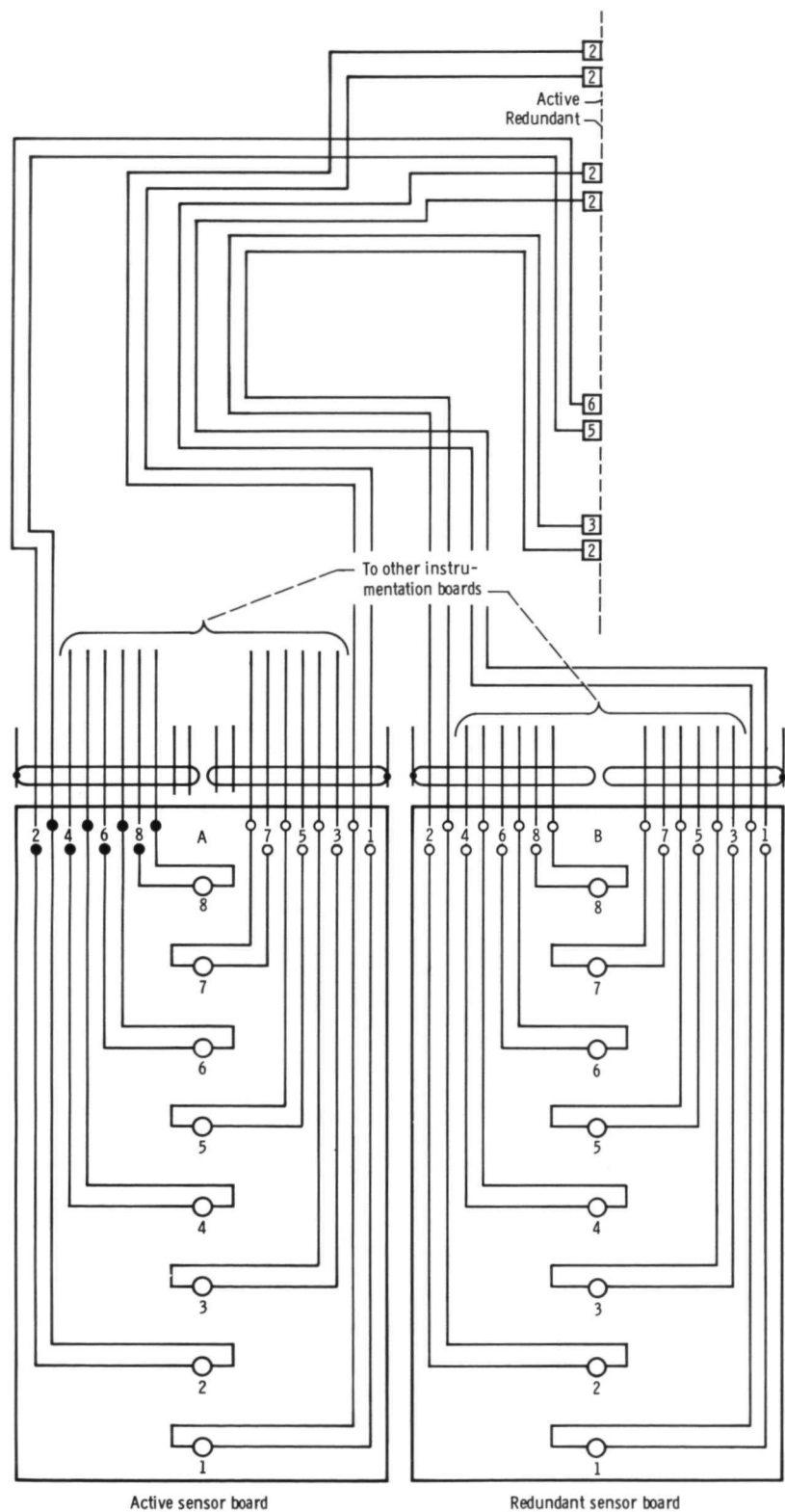


(a) Two sides of assembly apart.



(b) Two sides of reservoir sensor assembly fitted together.

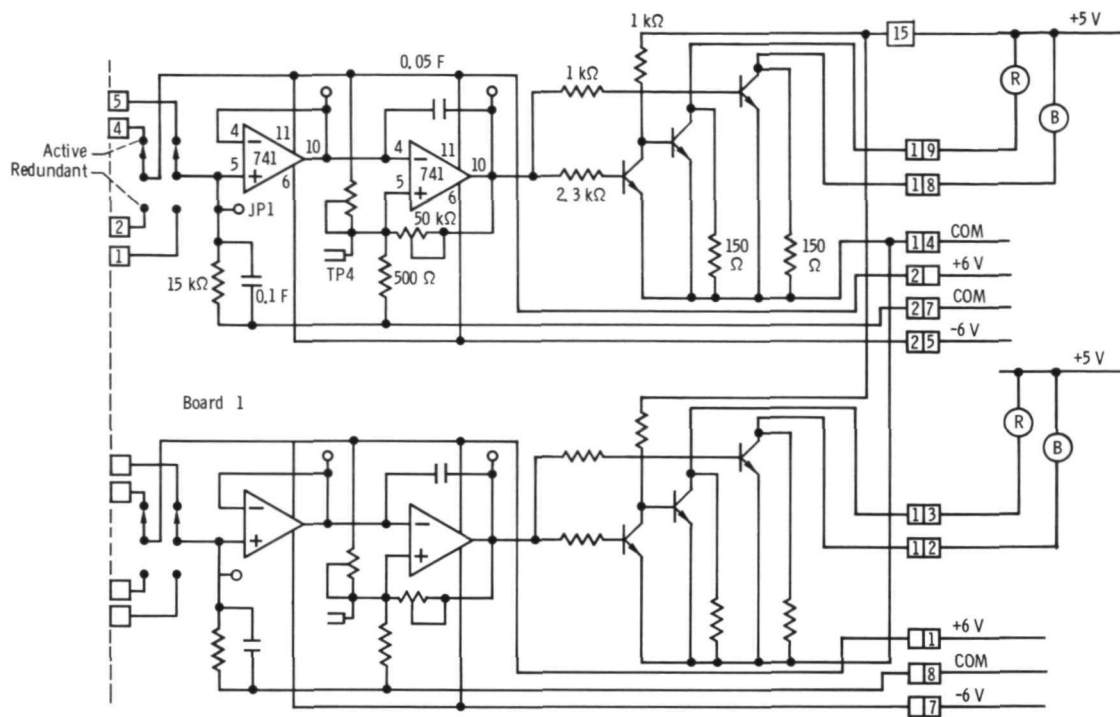
Figure 28. - Liquid-level sensors used in the liquid-helium reservoir.



CD-11509-25 Active sensor board

Redundant sensor board

Figure 29. - Circuit diagram of



CD-11509-25

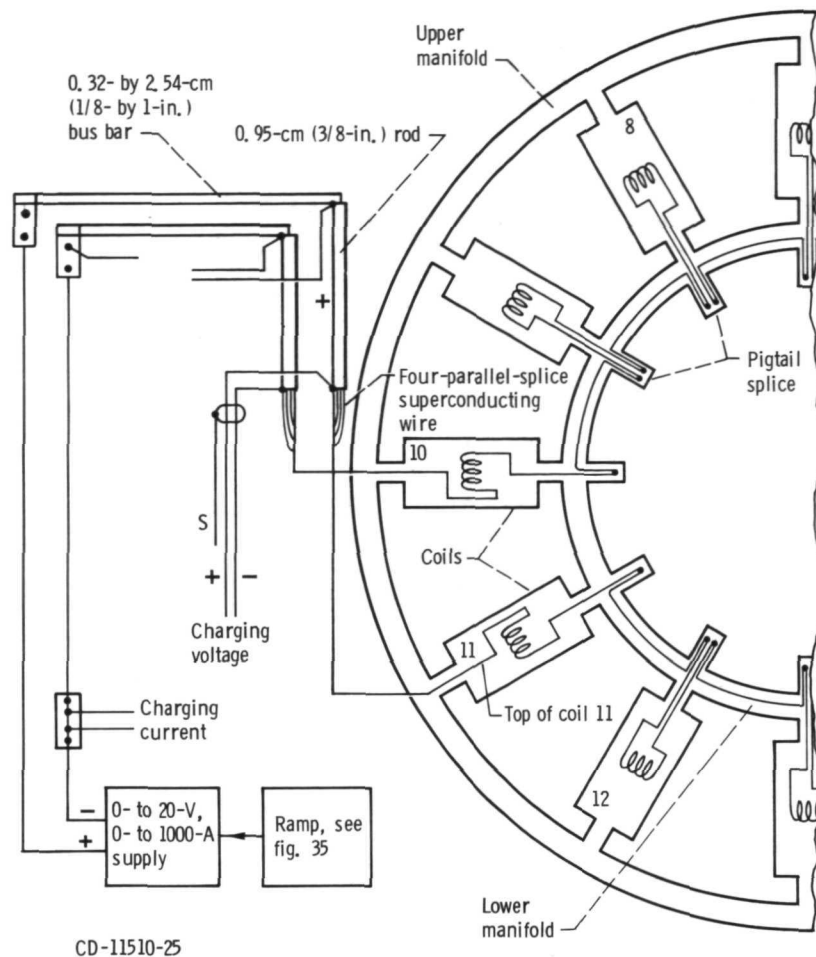
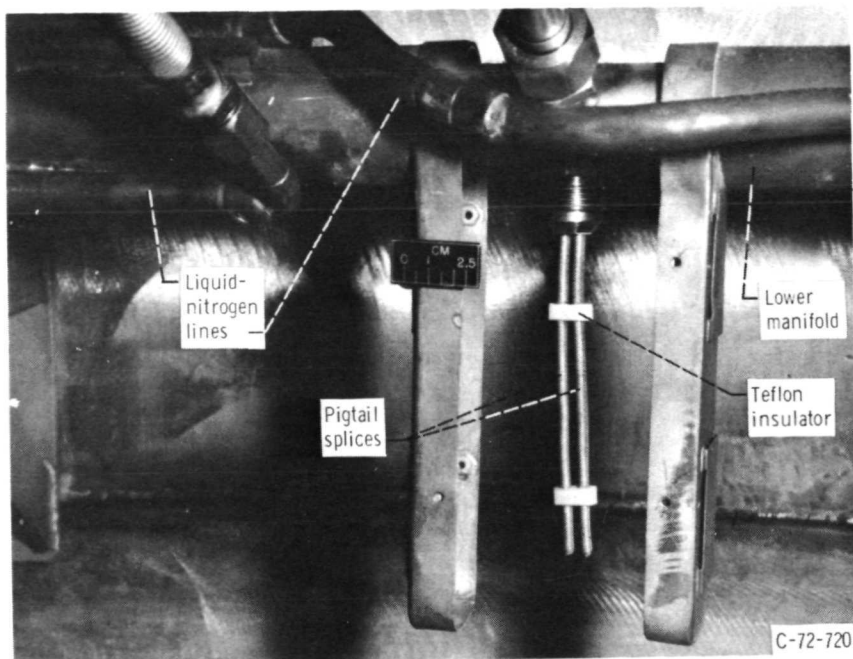


Figure 30. - Block diagram of coil connections and power supply.

The 12 coils are connected in series by splices in the superconducting wire. These splices are made in a pigtail assembly below each of the 12 coils. A typical pigtail assembly is shown in figure 31(a). Shown are two splices, each one of which consists of a lap splice of two wires. The series connections are such that the magnetic field is in the same direction in all 12 coils. A typical superconducting wire splice with round wire is shown in figure 31(b). Approximately 10 to 12 centimeters (4 to 5 in.) of the superconducting wire is cleaned of insulation. The wire is wrapped with tinned bare wire and the entire splice is soldered with indium solder.

Figure 32 is a sketch of the magnet leads and the manner of their connection from the coils to the terminals on the magnet lead termination box. The magnet leads from the coils are reinforced by a second parallel superconducting wire from the coil to the upper liquid-helium manifold. From this liquid-helium vent manifold to the bottom of the reservoir, each magnet lead consists of four parallel superconducting wires which are



(a) Actual pigtail assembly below one of 12 coils.



(b) Closeup of sample pigtail splice.

Figure 31. - Superconducting-wire splices.

attached to cylindrical copper bus bars 9.5 millimeters in diameter at the bottom of the liquid-helium reservoir tank. The two bus bars rise to the top of the reservoir tank and are attached to rectangular copper bus bars 25.4 by 6.35 millimeters in cross section. These rectangular bus bars then carry the current through the helium vent piping to the magnet lead termination box.

Figure 33 shows two views of the magnet lead termination box, which is located approximately 120 centimeters outside the vacuum tank along the liquid-helium vent line. Figure 33(a) is a top view of the magnet lead termination box with the two copper rods which carry the current to the coils. Figure 33(b) is a bottom view, looking at the underside of the magnet lead termination box with the bottom plate removed. Visible in figure 33(b) are the two rectangular bus bars in the vent line and the vertical copper rods which carry current to the power supply cables. Also visible in figure 33(b) is the bundle of liquid-level sensor cables which passes out through the vent line to the sensor lead termination box.

Figure 34 shows two views of the sensor lead termination box. Figure 34(a) is a top view of the termination box with the lid in place. Visible are the many multipin connectors required to bring the sensor leads to the room-temperature cable terminations. Figure 34(b) shows the sensor lead termination box with the lid removed. Visible are the 24

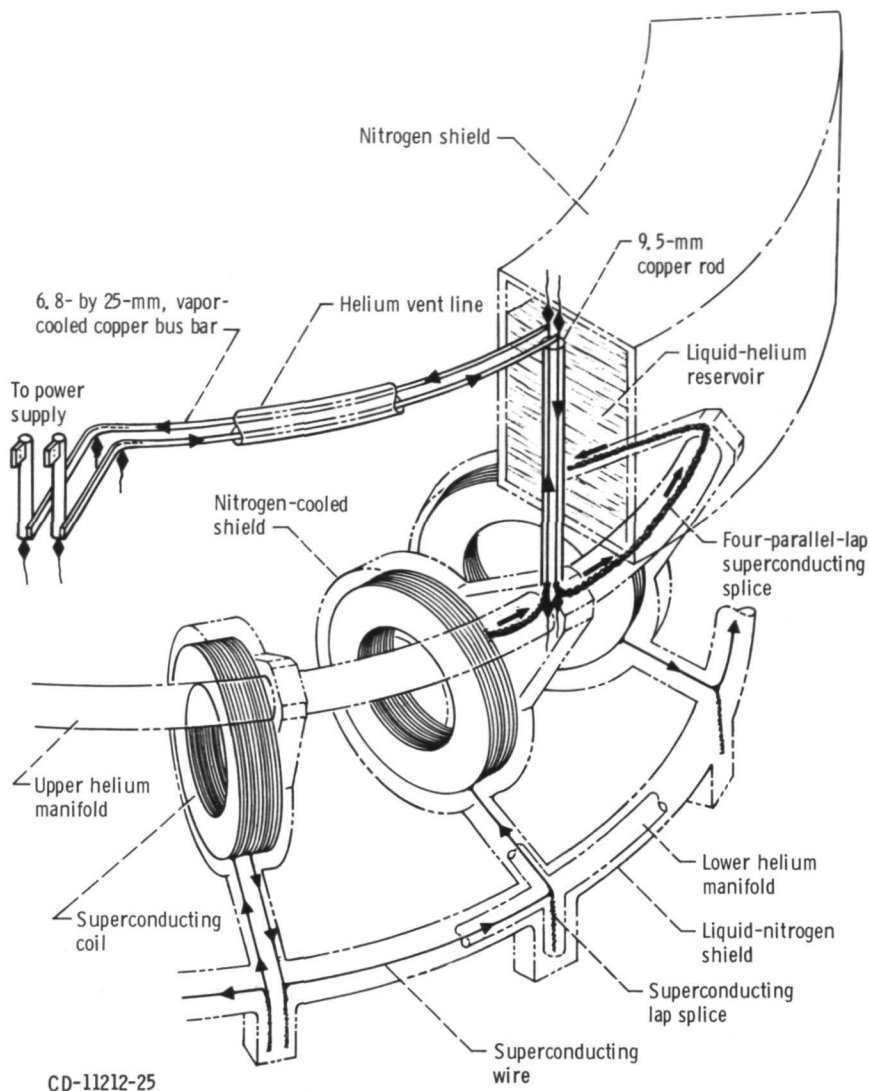
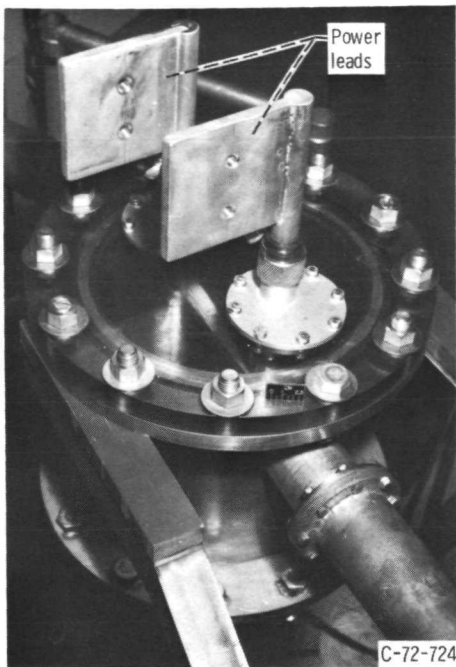


Figure 32. - Magnet leads and method of their connection from the coils to the room-temperature terminals at termination box.

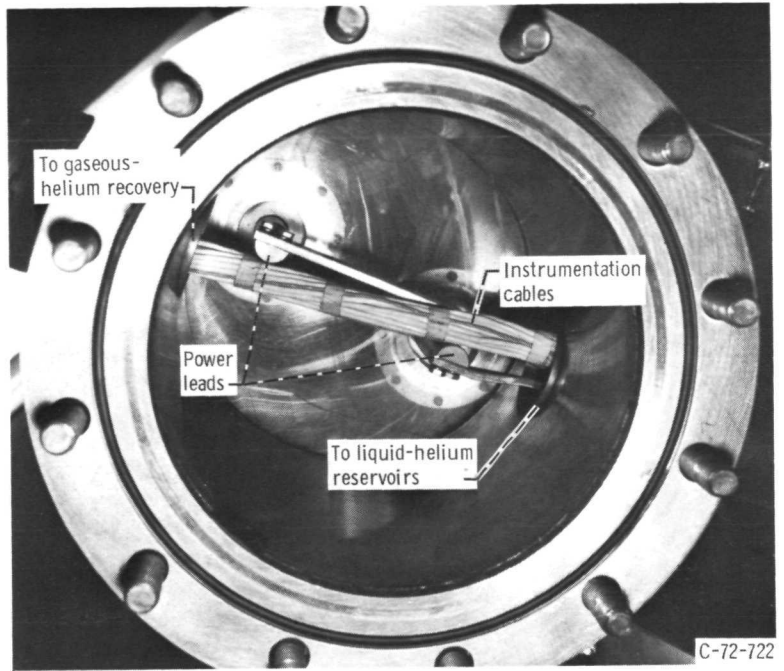
sensor lead cables required to connect the 96 individual germanium sensors and the 13 voltage taps which indicate charging voltages across individual coils and across the entire coil assembly.

The coil power supply has a capacity of 1000 amperes and 20 volts. This power supply is permanently connected to the coils, and current flows through the coils at all times when the magnets are charged. The power supply is controlled by a ramp-and-hold circuit which permits a programmed ramp rate to a preselected magnet current. A circuit diagram of the power supply ramp is shown in figure 35.

It was intended that the vacuum system of this facility operate unattended over nights and weekends. For this reason a comprehensive interlock system was used to shut the



(a) Magnet lead termination box seen from top.

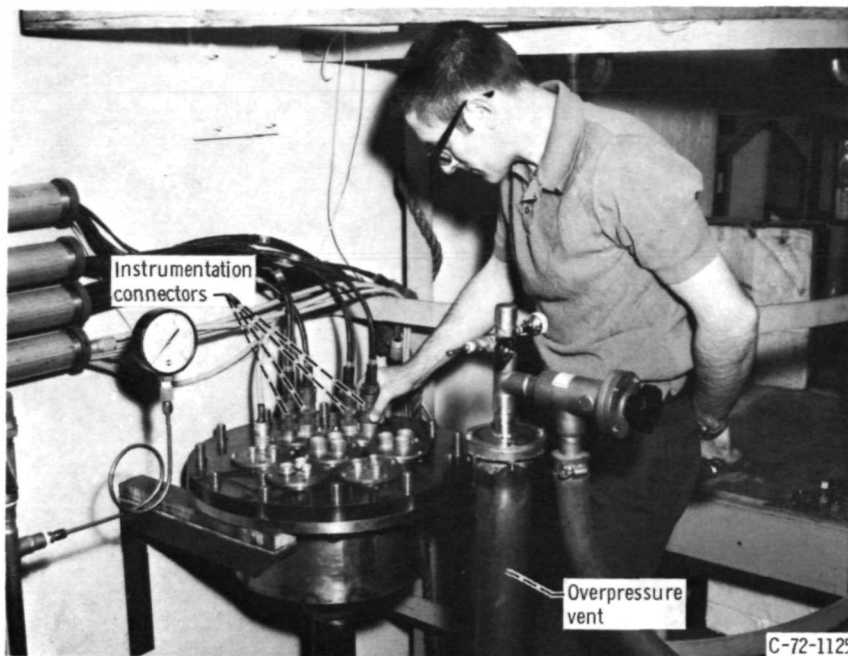


(b) Interior of magnet lead termination box seen from below with cover plate off.

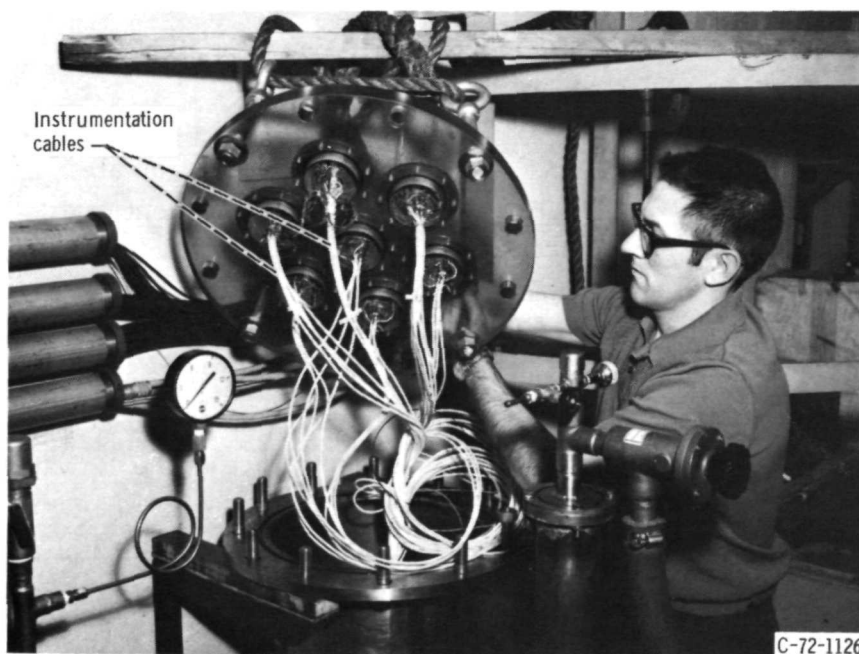
Figure 33. - Magnet lead termination box.

system down in the event of a failure of vacuum, power, water, or air. In addition to provisions to assure an orderly shutdown of the system in the event of a failure of the building services, a number of interlocks and protective circuits are associated with possible modes of failure during experimental operation. One of the most serious and most probable modes of failure during operation is the melting and rupture of one of the water-cooled anode rings. Such a rupture would lead to a rapid increase in tank pressure and freezing of water on the surrounding superconducting magnet Dewars, which are at liquid-nitrogen temperatures. The outlet water temperature of the 12 water-cooled anode rings is monitored with thermocouples. In the event that the exit cooling water temperature approaches the boiling point, or of a sudden rise in vacuum tank pressure, the anode ring water is shut off and the water remaining in the anode rings is purged by a high-pressure air system.

This facility contains 48 copper-constantan thermocouples placed in the liquid-helium and liquid-nitrogen portions of the system. These thermocouples are useful in monitoring the cooldown from room temperature and the heat load deposited on the system by the plasma.

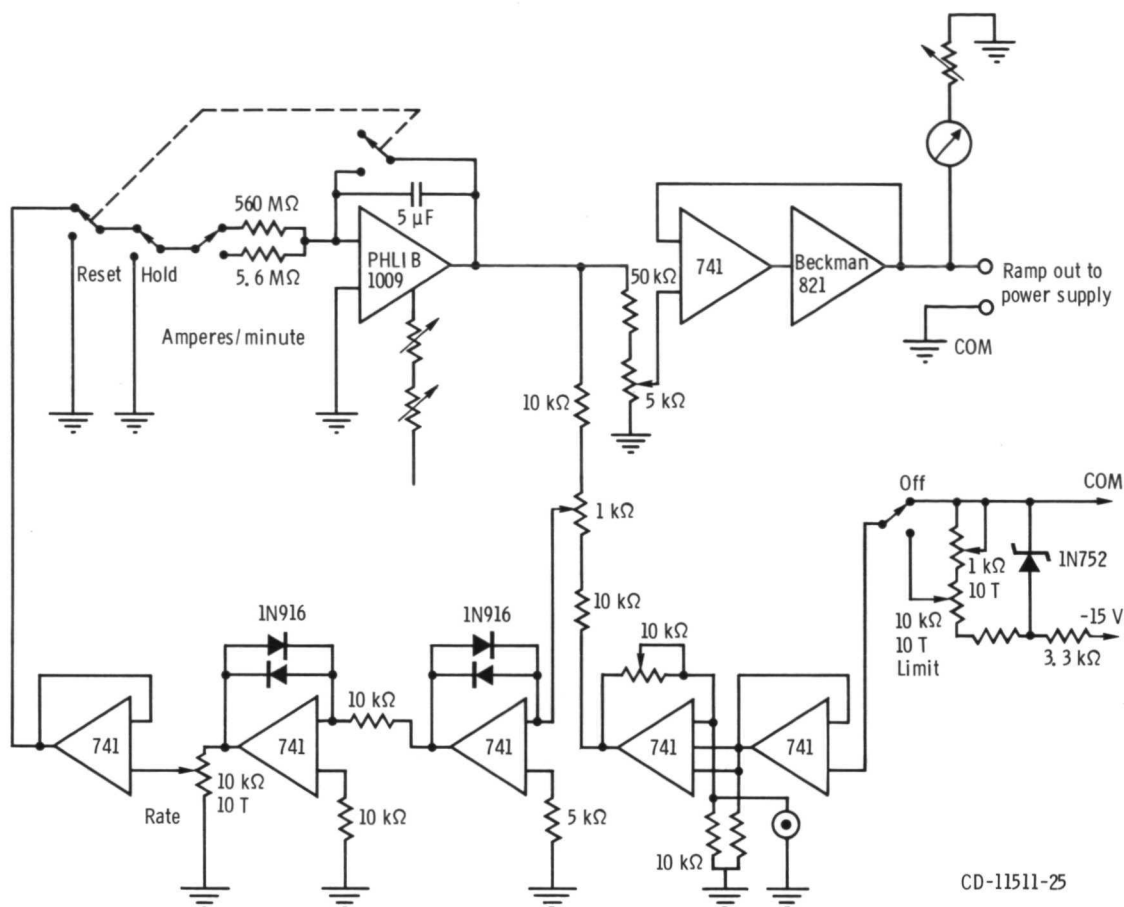


(a) Sensor lead termination box fully assembled.



(b) Sensor lead termination box with lid off.

Figure 34. - Sensor lead termination box.



CD-11511-25

Figure 35. - Circuit diagram of magnet power supply ramping circuit. (See also fig. 30.)

FACILITY APPEARANCE

An isometric cutaway drawing of the facility has been presented in figure 16. The facility, with the assembled coil array inside the vacuum tank before installation of the vacuum tank lid, is shown in figure 36. Evident in this figure is the very good access to the experimental volume by the pumping system, because the diffusion pump opening occupies the center portion of the toroidal array. Figure 37 shows the exterior of the vacuum tank. The catwalk which surrounds the upper portion of the tank is used to gain access to the airlocks through which the anode rings are inserted into the system. All the flanges not required for diagnostic instruments have mounted a glass viewport which consists of a 1.27-centimeter-thick X-ray-proof glass with laminated shatterproof safety glass on either side. Also visible in figure 37 are some of the twelve 15.2-centimeter-diameter ports on the bottom of the tank, which are aligned with the midplanes halfway between adjacent coils. Six of these 12 ports are required for liquid-nitrogen

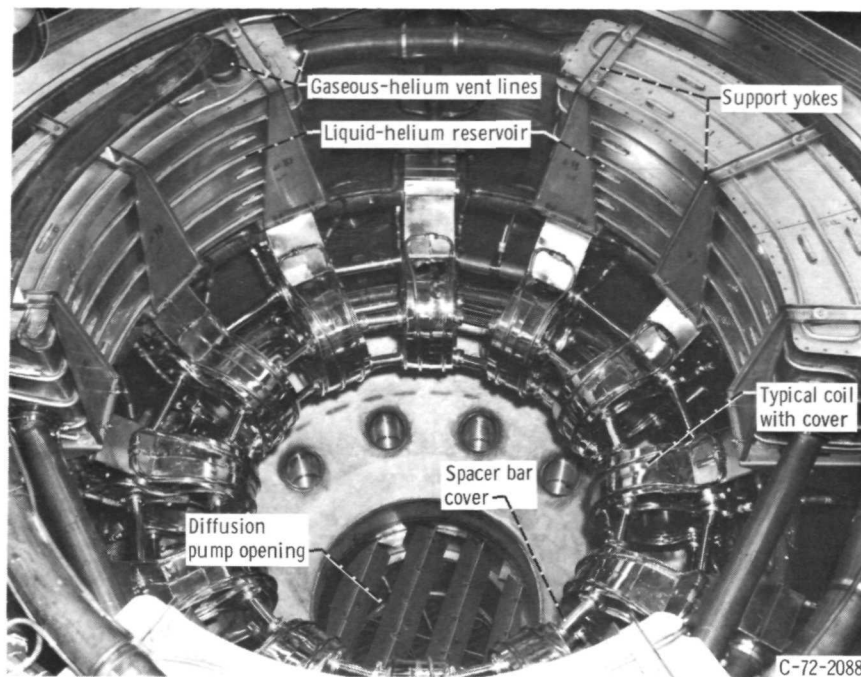


Figure 36. - Completely assembled coil array inside vacuum tank.

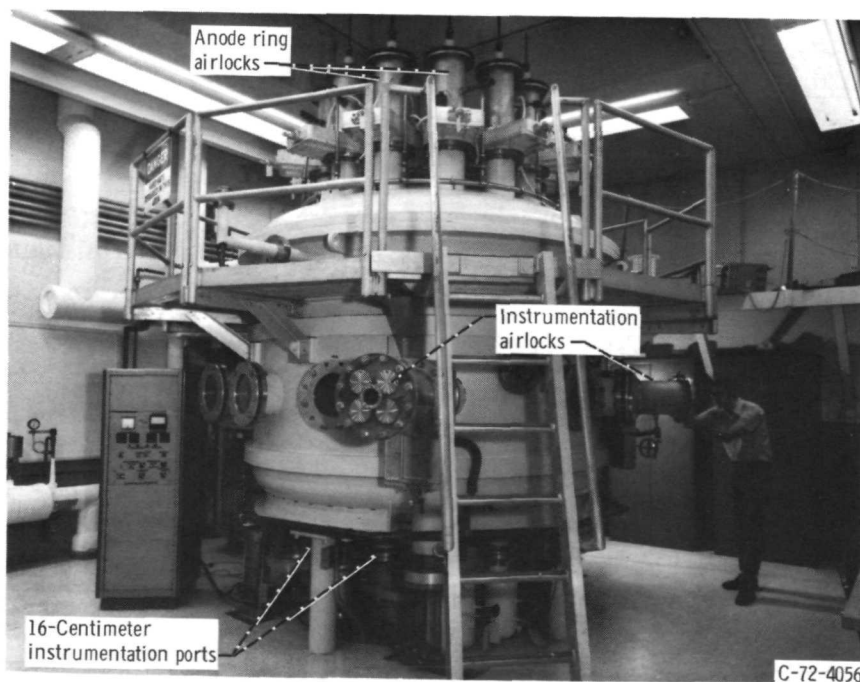


Figure 37. - Exterior of vacuum tank.

service lines and other service equipment. Six of the 12 positions are available for the insertion of probes through the bottom of the tank. There are airlocks on three of these six ports.

Figure 38 shows the control room instrument racks which control the vacuum and magnet systems. On the instrumentation rack on the far left is the main control and monitoring board for the vacuum system. The second instrument rack from the left contains, on the top, the liquid-level indicators for the three reservoirs; and immediately below are the high- and low-level indicators for the 12 superconducting coils. Immediately below the sensor indicating lights are 12 voltmeters which indicate the charging voltage across each of the 12 coils.

Figure 39 is a floor plan of the facility. Experiments are normally conducted on the upper level surrounding the vacuum tank. When direct operation is not possible because of a high neutron or X-radiation field, the experiment can be operated remotely from the control room on the first floor. The walls surrounding the experiment room are 30-centimeter-thick concrete, and the floor is 23-centimeter-thick concrete. Immediately under the vacuum tank are the power supplies for the coils, a high-voltage power supply required for the anode rings, the forepump, the diffusion pump, and other auxiliary systems required to operate the facility. A 5-ton bridge crane is available to manipulate the lid of the vacuum tank and other heavy system components. There is an approximately 2.6-meter-square hatch in the floor of the experiment level through which instruments can be raised and lowered as needed.

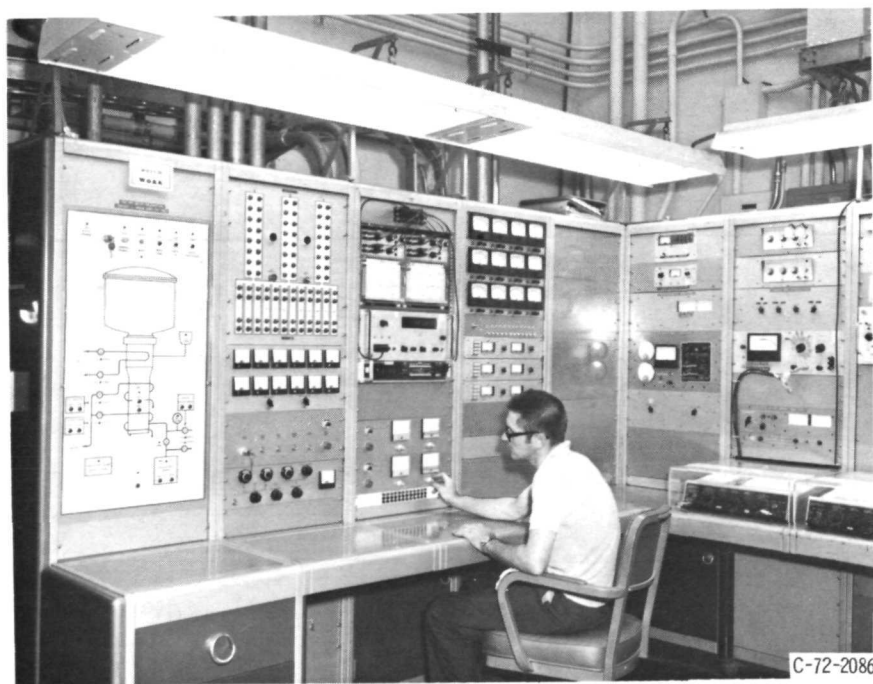


Figure 38. - Control room racks which contain instrumentation for magnetic facility.

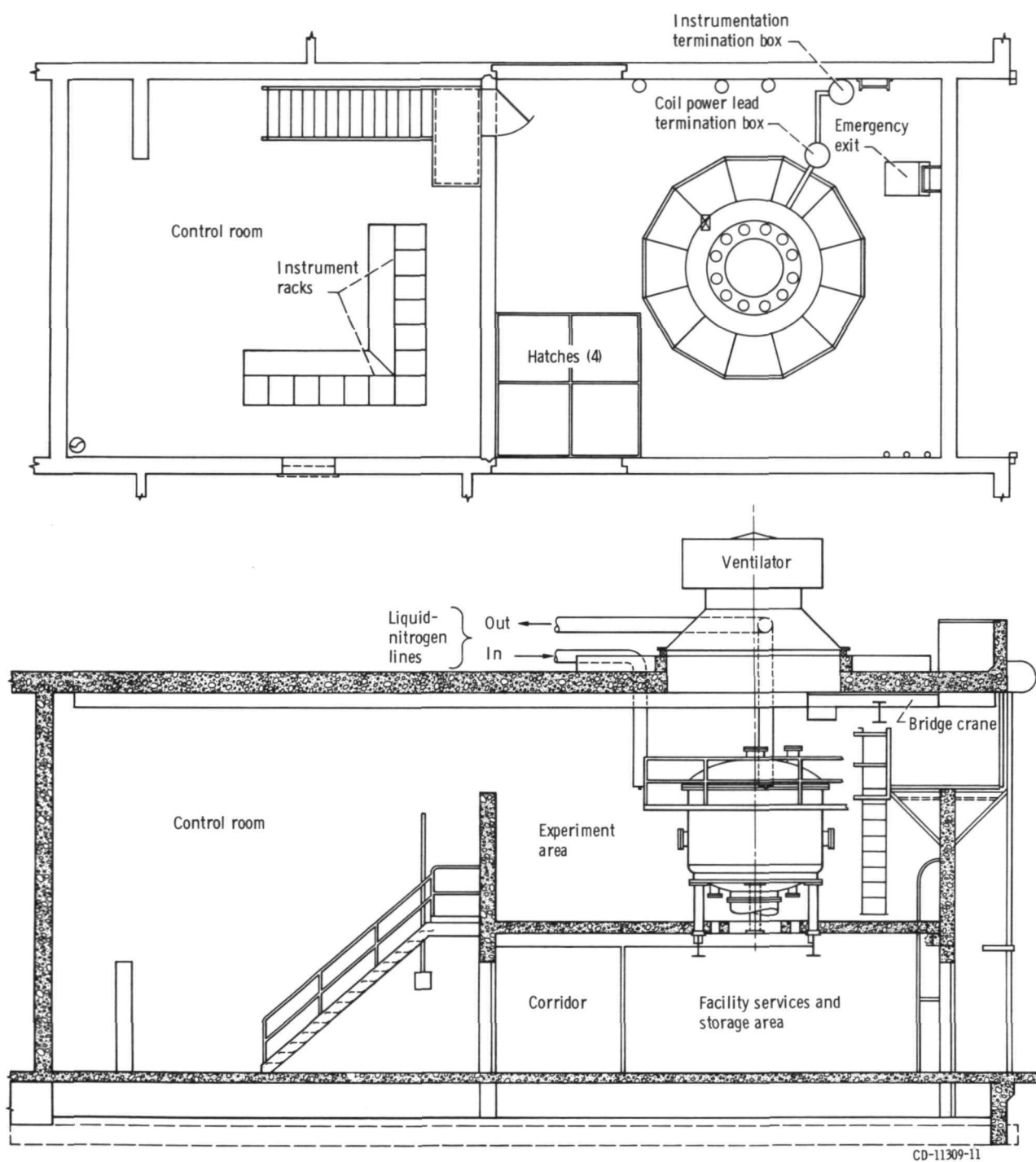






Figure 39. - Plan and elevation of superconducting bumpy-torus magnet facility.

FACILITY PERFORMANCE

Superconducting Coil Performance

Each of the 12 coils was individually tested and met or exceeded its design current before being incorporated in the facility. The performance of these coils during their individual tests is summarized in table II. Shown are the location of each coil, the type of wire used (whether round or square), the number of turns in the coil, the range of charging rates utilized during the coil tests, and the maximum current at which the coil remained superconducting for at least 5 minutes. The coils met or exceeded their design current of 700 amperes for charging rates that ranged from 75 to 180 amperes per minute. Also notable in table II is the very high uniformity of the number of turns, which

TABLE II. - INDIVIDUAL COIL PERFORMANCE

Coil	Position in toroid, deg	Wire type	Number of turns on coil	Charging rate range, A/min	Maximum hold- ing current, A
1	0	Round	977	45 to 240	750
2	30	Square	977	90 to 450	800
3	60		977	50 to 250	800
4	90		974	120 to 500	800
5	120		977	60 to 180	750
6	150			30 to 240	750
7	180			60 to 180	752
8	210			30 to 180	755
9	240	Round		45 to 240	750
10	270			40 to 460	850
11	300			45 to 240	850
12	330		977	45 to 240	852

was made possible by the skill of the coil-winding crew. The departure from field uniformity attributable to variations in the number of ampere turns per coil should be less than ± 0.3 percent in this array of 12 coils. A preliminary test of a canted pair of superconducting coils showed that the particular pair of square-wire coils used was capable of 800 amperes before going normal.

The result of testing the superconducting coil performance for the entire array was that the entire array could be held at a maximum magnetic field on the magnetic axis of 3.23 teslas for at least an hour; the design magnetic field was 3.00 teslas. Figure 40 is a survey of the magnetic field across the plane of the torus midway between two adjacent

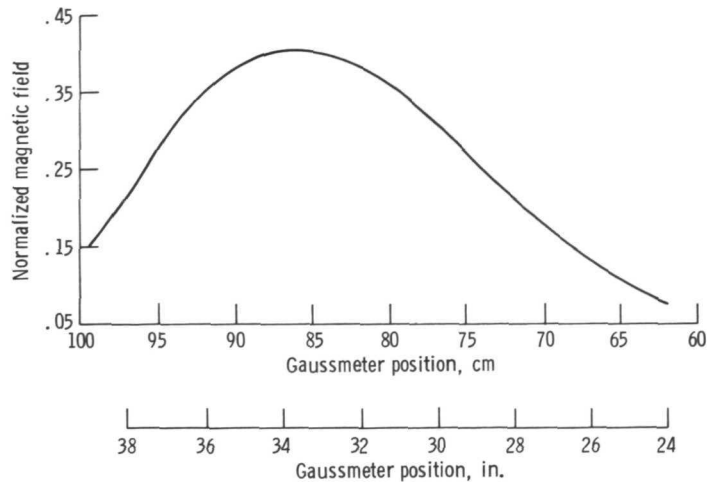


Figure 40. - Measured magnetic field as a function of radius in midplane between two coils, normalized to a relative magnetic field of 0.403 on the magnetic axis.

coils, normalized to a relative field of 0.403 on the magnetic axis. There is agreement to within 3 percent with the numerical computations presented in figure 11.

It was found that the facility went normal at a magnetic field of 3.35 teslas. Figure 41 is a plot of the magnet current and total voltage drop during a coil normalcy. It takes approximately 100 seconds for the energy of the magnetic field to dissipate and the coil current to go to zero. It takes somewhat longer than this for the energy to appear in the venting helium gas. About 0.014 cubic meter (14 liters) of liquid helium were boiled off during a magnet chargeup at 90 amperes per minute, and 0.14 cubic meter (140 liters) were boiled off during a normalcy near the design field of 3.0 teslas. Approximately 0.21 cubic meter (210 liters) were boiled off during a normalcy at a field of 3.35 teslas. It was found that this facility would achieve its design magnetic field over charging rates from 30 to 210 amperes per minute, although a normalcy during chargeup was least likely over the range from 90 to 150 amperes per minute. Over this charging rate range, it took from 7.0 to 4.2 minutes to charge the coils to their rated magnetic field of 3.0 teslas at 630 amperes. An approximate boundary for superconducting operation of this facility is shown in figure 42, in which the limiting value of the rise rate is shown as a function of the normal current.

Mechanical Performance

With equal currents in all coils, the magnetic forces acting on a coil will be very nearly in equilibrium because of the equal and opposite forces on adjacent coils. Because the 12 coils are tilted with respect to each other by 30° in this toroidal array, the

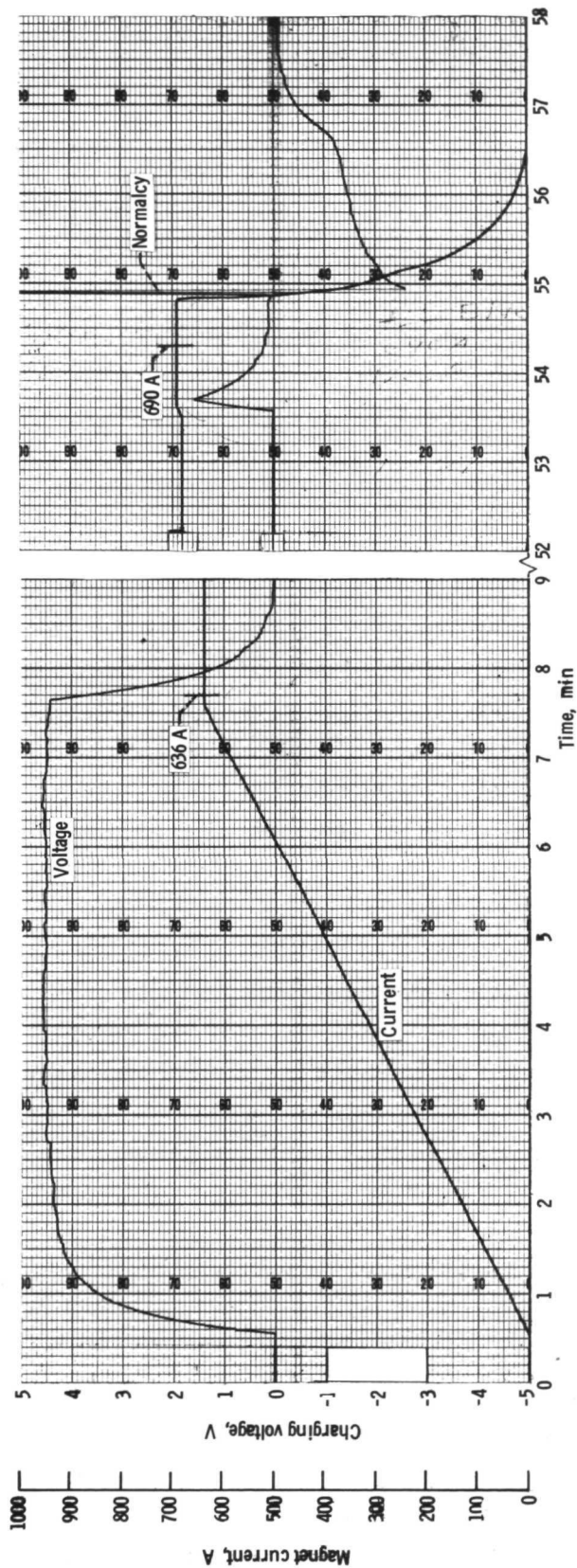


Figure 41. - Raw data showing magnet current and voltage during a charging and normalcy.

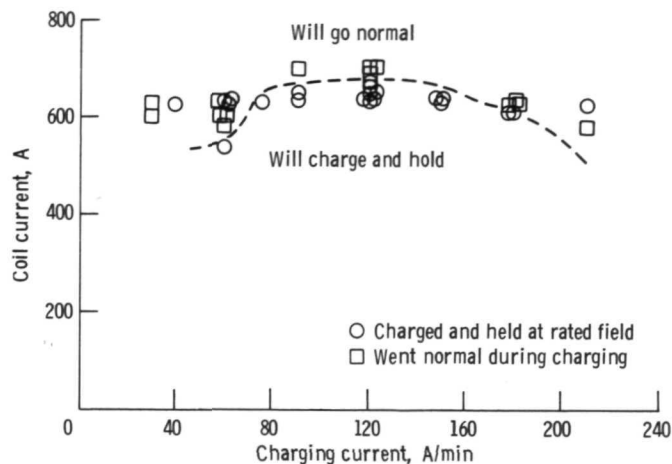


Figure 42. - Magnet charging rate as function of maximum coil current achievable with that ramping rate. Magnet facility can be charged at any rate below boundary indicated in this figure.

result will be a small compressive force tending to draw the 12 coils to a smaller major radius. The worst possible disposition of mechanical forces that can arise in this facility occurs when a few adjacent coils have superconducting currents flowing in them. In order to test the mechanical and cryogenic design of the facility before the entire assembly was put together, a coil pair test was performed in another vacuum tank with a canted pair of coils.

Figure 43 shows the coil pair test rig. The major radius of curvature of this test rig was identical to that on the completed facility. Two of the coils and liquid-nitrogen can covers used in the final facility were used in this test. The spacer bars on the outside of the two coils were used to brace the coil pair assembly against the walls of the 1.5-meter-diameter vacuum vessel in which the test was performed. The coils were connected to an upper and lower liquid-helium manifold. The reservoir was substantially different in design from those used in the facility. The two coils in the configuration shown in figure 43 have nearly the maximum possible compressive forces acting between them and, hence, provide a test case of the spacer bars and the other structural elements of the coil assembly. These two coils were energized to a current of 800 amperes and were able to hold this current for more than 5 minutes without plastic deformation or failure.

The coil pair assembly shown in figure 43 contained 13 AN fittings at liquid-helium temperatures. These fittings had their mating surfaces prepared and were torqued in the manner described previously. In the coil pair test there were no leaks from the liquid-helium system into the vacuum tank during the cooldown process, during the coil charge-up, or during the coil normalcy when there was a backpressure in the system. Possible

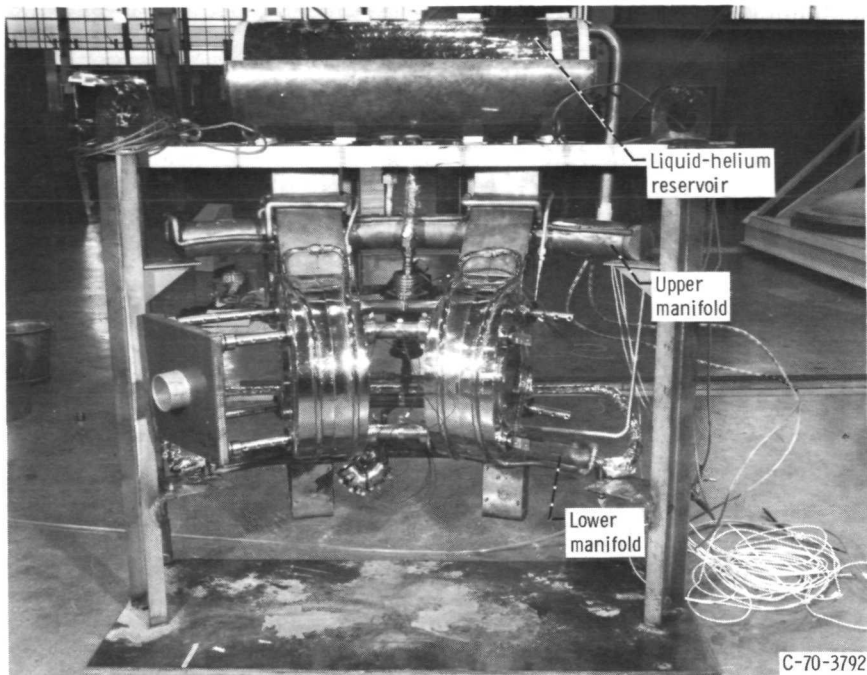


Figure 43. - Coil pair test rig which was designed to test mechanical and cryogenic performance of facility design.

leaks of helium into the vacuum system were monitored by a leak detector on its most sensitive scale. This indicated no helium leak whatever into the vacuum tank during the test.

The only feature of the mechanical performance of the 12-coil array which could not be adequately simulated in the coil pair test was the stability behavior of the ring of 12 coils with the magnetic forces acting between the 12 coils. It was considered possible that the array of 12 coils, in spite of the spacer bars, and in spite of the rigidity of the upper liquid-helium manifold to which the assembly is attached, might be subject to a form of torsional instability which is illustrated by an O-ring which can be folded from a single hoop into a three-turn hoop. In order to monitor the stability of the coil array, a system was used that was very similar to that used to monitor the flutter stability of airplane wings without destroying the aircraft. This system consisted of strain gages which were capable of operating at liquid-helium temperatures and were mounted on one of the outer spacer bars. A pivoted hammer was installed to deliver a fixed impulse to a spacer bar, which excited the elliptical modes of oscillation of the entire coil array. As the coils were charged up for the first time, the magnet current was increased, in increments of 50 amperes, to the design limit. At each 50-ampere increment, an impulse was given to the coil array. The elliptical mode vibrations induced in the coil array were observed with an oscilloscope connected to the strain gages.

If the system is stable, the oscillations induced by the impulsive blow will die away, yielding an exponentially decreasing oscillation waveform. If, however, the system is neutrally stable, the oscillations will continue undamped after the impulsive loading. If the system is unstable, the oscillations will grow until the magnet assembly collapses. At each 50-ampere increment, the effective decay constant of the impulsively induced oscillations was measured. Figure 44 shows oscillographs of the response of the magnet system to an impulsive excitation for magnet currents ranging from 350 to 625 amperes.

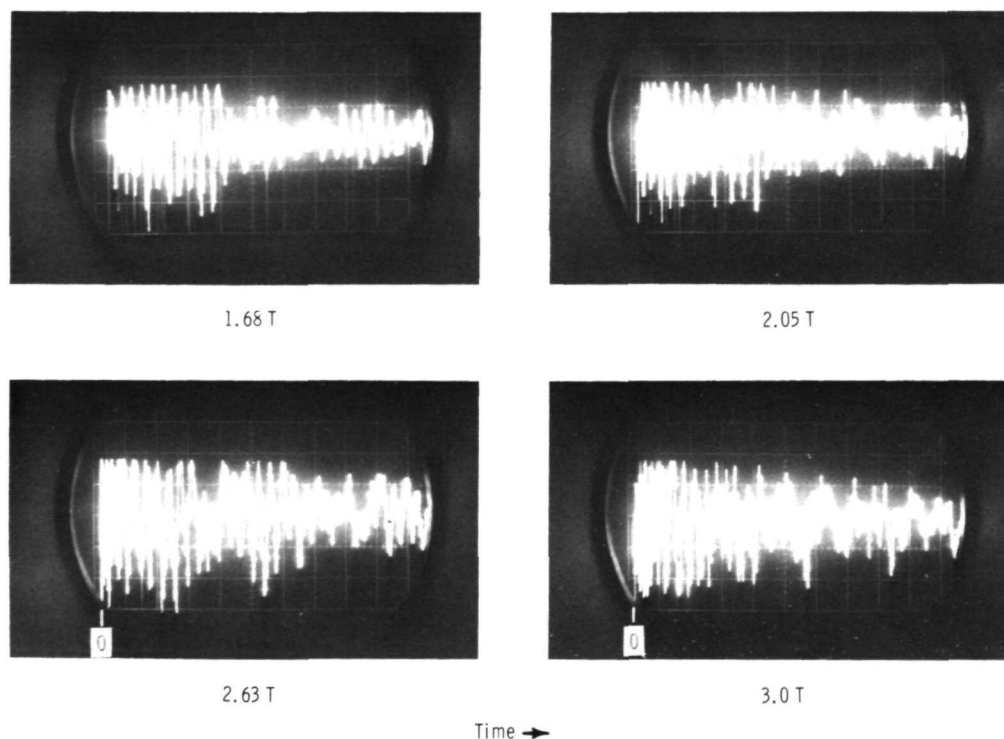


Figure 44. - Response of the magnet system to an impulsive excitation for various values of maximum magnet field in teslas. Note the exponentially decreasing wave forms.

Each of the oscillographs similar to figure 44 had a characteristic e-folding decay constant α given by the formula

$$A = A_0 e^{-\alpha t}$$

This decay constant was plotted as a function of magnet field as the magnets were charged. So long as α is positive, this implies an exponentially decaying waveform similar to that in figure 44, and the magnet facility is stable at that magnet current. If the value of α decreases and extrapolates to zero somewhere in the designed range of

operating currents, the magnet facility is unstable. As shown in figure 44, however, the value of α is constant and the system is stable over the intended range of operating conditions. This point is significant for future design of facilities of this nature. It suggests that this design can be scaled to larger sizes and stronger magnetic fields with a reasonable expectation that the present system of four spacer bars between the magnet spool-pieces will be stable without support from additional structural members, provided that the structures are capable of bearing the magnetic forces.

Cryogenic System Performance

The liquid-nitrogen system and the coils were cooled from room temperature to liquid-nitrogen temperature by evacuating the large vacuum tank and turning on the liquid nitrogen. The temperature of the liquid-nitrogen system was monitored with thermocouples at several locations. The results of the cooldown are shown in figure 45. The two cooldown curves represent two different locations in the liquid-nitrogen system: one of the 12 coil covers and the midpoint of a long spacer bar shield. As shown, it took approximately 15 minutes for the spacer bar shield to reach liquid-nitrogen temperature.

When the liquid-nitrogen system was at liquid-nitrogen temperature, the facility was allowed to cool off for 24 hours, at which time the liquid-helium system reached a temperature of approximately 233 K. The liquid-helium system was taken from 233 K to liquid-helium temperature by the passage of liquid helium through the system. Approx-

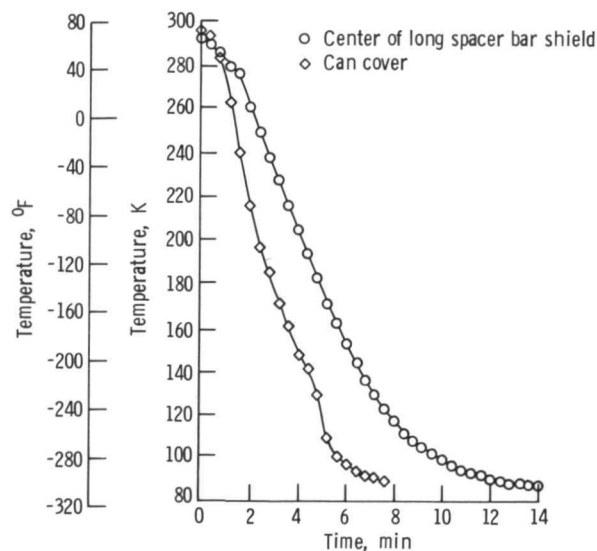


Figure 45. - Temperatures of liquid-nitrogen can covers as function of time during cooldown from room temperature to liquid-nitrogen temperature.

imately 20 minutes were required to cool the coils from 233 K to liquid-nitrogen temperature, and an additional 60 minutes before liquid helium began to accumulate in the system. It is estimated that the total amount of liquid helium required to cool the system from 233 K to liquid-helium temperatures was approximately 2.3 cubic meters (2300 liters).

Figure 46 is a block diagram of the apparatus used to measure the liquid-helium boiloff. This apparatus consists of a bypass in the liquid-helium vent line in which the venting helium gas passes through a heater and through a rotometer which measures the

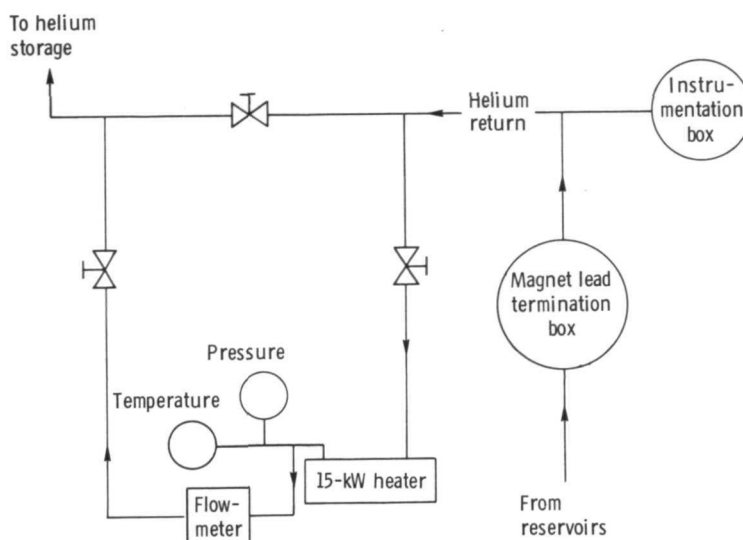


Figure 46. - Block diagram of apparatus used to measure boiloff rate of helium from the facility.

integrated gas flow through the system. The steady-state liquid-helium boiloff rate was measured with the reservoirs initially filled when the system seemed to be equilibrated, both with and without the coils charged. The boiloff rate without the coils charged was 0.087 cubic meter (87 liters) per hour of liquid helium. With the coils charged to a maximum field on the magnetic axis of 2.40 teslas, the boiloff rate was 0.095 cubic meter (95 liters) per hour. The boiloff rate, when the coils were charged to their rated field of 3.0 teslas, was 0.1 cubic meter (100 liters) per hour. The boiloff of the system was measured during the charging of the coils. These started with no current and ended at the rated field strength of 3.0 teslas. The boiloff, over and above the constant thermal leakage, was 0.014 cubic meter (14 liters) for the charging process, at a ramp rate of 90 amperes per minute.

The backpressure in the system was measured during a coil normalcy which took place at 3.30 teslas. It was found that the pressure at the top of the liquid-helium reservoirs was $1.18 \times 10^5 \text{ N/m}^2$ (17.2 psia). When the first coil in the system went normal,

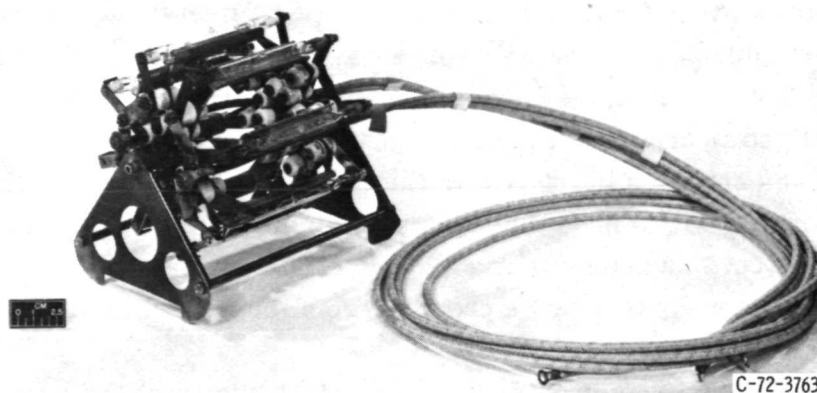


Figure 47. - Array of quartz lamps used to deposit a known amount of radiant energy on inner bore of one of the 12 coils.

this triggered six other coils to go normal. The facility has undergone 24 coil normalcies at the present writing. No apparent damage or degradation of performance of the coils occurred as a result of the coil normalcies.

The effectiveness of the liquid-nitrogen can covers in carrying away radiant energy was measured with the radiant heat loading assembly shown in figure 47. This assembly consisted of eight quartz lamps which were energized with a variable transformer and could irradiate the inner bore of one of the 12 superconducting coils with as much as 3 kilowatts of radiant power. We wanted to see at what point vapor lock would occur in the liquid-nitrogen cooling passages on the inner bore of this coil, shown in figure 21, and also to see how much of the radiant energy eventually appeared in the liquid-helium canister. Figure 48 is a graph of the temperature at the midpoint of the inner bore of the liquid-nitrogen-temperature shield of this coil as a function of time and of the radiant energy deposited on the system. The fluctuations in temperature are probably caused by

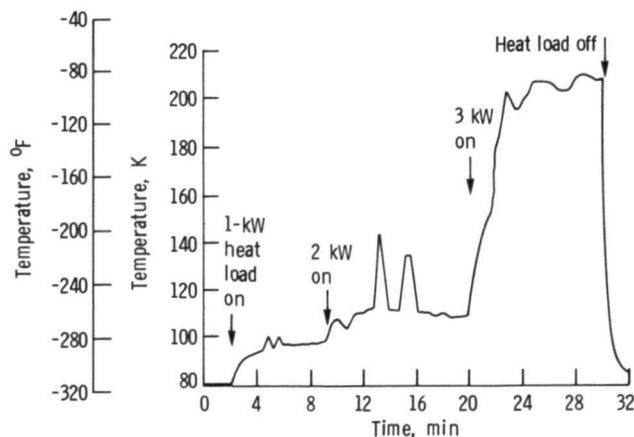


Figure 48. - Temperature of center point of bore of liquid-nitrogen heat shield as function of time and heat load.

film boiling or vapor lock. No difference in the boiloff rate of liquid helium was noted, even with 3-kilowatt loading on the inner bore of the liquid-nitrogen heat shield.

Performance of the AN fittings was measured by monitoring the background partial pressure of helium, oxygen, and nitrogen in the vacuum tank at room temperature as the liquid-helium system was cooled down, as it was filled with liquid helium, as the magnets were charged, and finally as the magnets went normal. The performance achieved in the coil pair test was repeated in the test of the facility as a whole. At the present writing the system has undergone three thermal cycles from room temperature to liquid-helium temperature, 24 coil normalcies, and 40 cycles of charging and discharging the coil assembly without any serious leakage problem from the fittings in either the liquid-nitrogen or liquid-helium systems.

A significant effort was required to eliminate leaks from the liquid-nitrogen and liquid-helium systems into the vacuum tank in which they were enclosed. In the liquid-nitrogen system, nearly all leaks were associated with silver solder joints which were made with an improper technique or with copper welds in the liquid-nitrogen can covers. In the liquid-helium system, the leaks were associated with stainless-steel welds or with stainless-steel bellows which were pitted by corrosion caused by silver solder flux. The AN fittings in both systems presented no leakage problems.

With all components of the system at room temperature (except the liquid-nitrogen cold trap above the diffusion pump), the leakage from the liquid-nitrogen system into the vacuum tank contributed a partial pressure of less than 5×10^{-10} torr to the tank background pressure. Leakage from the room-temperature liquid-helium system into the tank contributed less than 3.5×10^{-9} torr to the background pressure. With liquid helium in the liquid-helium system, the leakage of helium from it contributed a partial pressure of less than 2×10^{-8} torr.

Vacuum System Performance

During the final shakedown tests the background pressure of the system with all coil components at room temperature was 4.5×10^{-7} torr. When both the liquid-nitrogen and liquid-helium systems were at liquid-nitrogen temperature, the background pressure of the vacuum system was reduced to 3.8×10^{-7} torr. When the liquid-helium system was taken to liquid-helium temperature, additional cryopumping reduced the ultimate background pressure of the system to 2.2×10^{-7} torr. These measurements were made with the pumping speed controller in the open position. After a small air leak was fixed, the ultimate pressure with the tank warm was 1.6×10^{-7} torr.

The effect of the pumping speed controller can be seen in figure 49(a), which shows the background pressure of the vacuum system as the angle of the flaps in the pumping

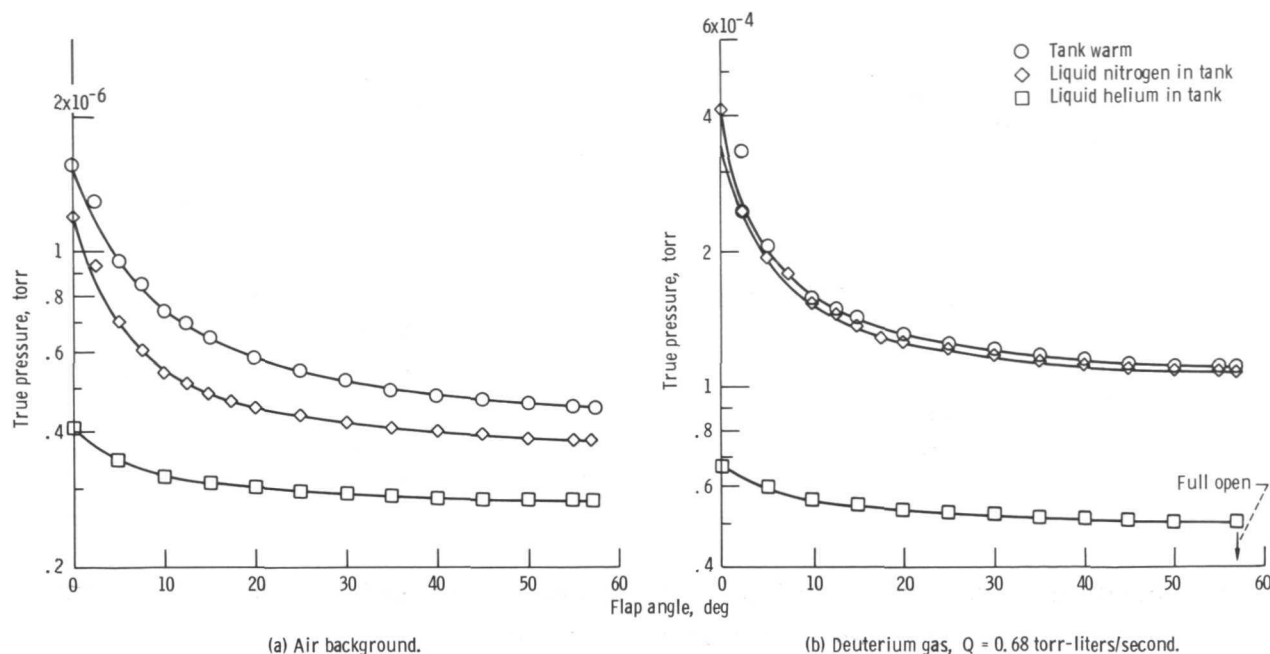


Figure 49. - Effect of pumping speed controller, pumping pressure as function of flap angle.

speed controller is changed. The calibrations on the x-axis represent the angle of the flaps with respect to the horizontal. Figure 49(b) shows the true tank pressure as a function of flap angle with a constant throughput of deuterium gas. The effect of the incremental pumping speed caused by cold cryogenic surfaces in the vacuum tank can be seen.

The partial pressure of background contaminants was monitored with a mass spectrometer, and it was found that the principal contaminants were about equally divided between air and water vapor with the components in the tank at room temperature. With the coils charged to 3.0 teslas, the background consisted of 90-percent air and 10-percent helium gas.

Figure 50(a) shows the effective pumping speed of the system with air and with and without cryogenics in the tank. Figure 50(b) shows the pumping speed of the system with deuterium gas.

Performance of Instrumentation and Electrical Systems

The liquid-helium sensors performed quite satisfactorily. Of the 96 liquid-helium level sensors, it was found that five were open-circuited immediately before the system was cooled down to cryogenic temperatures for the first time. These open circuits may have resulted from mechanical shock or vibration during the assembly or welding process. After the system experienced one thermal cycle from room temperature to liquid-

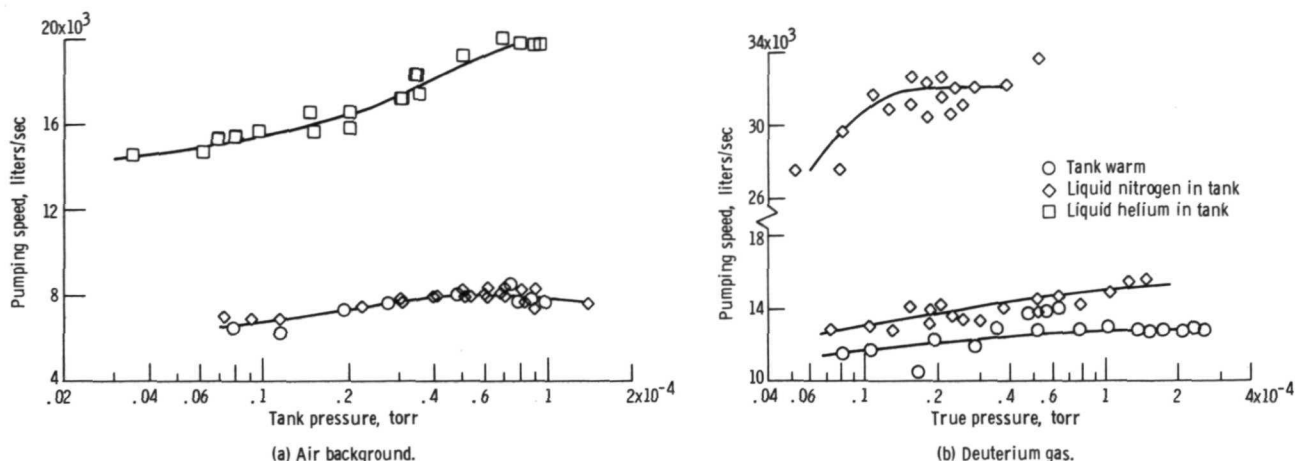


Figure 50. - Effect of pumping speed controller, pumping speed as function of tank pressure.

helium temperature, two additional liquid-helium sensors showed an open circuit. However, because a redundant liquid-helium level sensor was available to each location, all 48 stations indicated the liquid-helium level. No additional sensors have failed as of the present writing.

The performance of the coil power supply was quite satisfactory. It ramped up to the rated field and down automatically and produced no unanticipated behavior during the coil charging process.

Lewis Research Center,
 National Aeronautics and Space Administration,
 Cleveland, Ohio, April 26, 1973,
 503-10.

REFERENCES

1. Roth, J. Reece; Rayle, Warren D.; and Reinmann, John J.: Technological Problems Anticipated in the Application of Fusion Reactors to Space Propulsion and Power Generation. NASA TM X-2106, 1970.
2. Roth, J. R.; Rayle, W. D.; and Reinmann, J. J.: Fusion Power for Space Propulsion. New Scientist, vol. 54, no. 792, Apr. 20, 1972, pp. 125-137.
3. Roth, J. Reece; Freeman, Donald C., Jr.; and Haid, David A.: Superconducting Magnet Facility for Plasma Physics Research. Rev. Sci. Inst., vol. 36, no. 10, Oct. 1965, pp. 1481-1485.

4. Roth, J. Reece: Plasma Stability and the Bohr-van Leeuwen Theorem. NASA TN D-3880, 1967.
5. Roth, J. Reece: Optimization of Adiabatic Magnetic Mirror Fields for Controlled Fusion Research. NASA TM X-1251, 1966.
6. Coles, W. D.; Laurence, J. C.; and Brown, G. V.: Cryogenic and Superconducting Magnet Research at the NASA Lewis Research Center. Paper 21c, 62nd Annual Meeting of the AIChE, Washington, D.C., November 16-20, 1969.
7. Laurence, James C.: Superconductive Magnets. Proceedings of the Helium Symposium, Washington, D.C., March 23-24, 1970, J. S. Blizin, Ed., pp. 182-200.



POSTMASTER: If Undeliverable (Section 158
Postal Manual) Do Not Return

"The aeronautical and space activities of the United States shall be conducted so as to contribute . . . to the expansion of human knowledge of phenomena in the atmosphere and space. The Administration shall provide for the widest practicable and appropriate dissemination of information concerning its activities and the results thereof."

—NATIONAL AERONAUTICS AND SPACE ACT OF 1958

NASA SCIENTIFIC AND TECHNICAL PUBLICATIONS

TECHNICAL REPORTS: Scientific and technical information considered important, complete, and a lasting contribution to existing knowledge.

TECHNICAL NOTES: Information less broad in scope but nevertheless of importance as a contribution to existing knowledge.

TECHNICAL MEMORANDUMS: Information receiving limited distribution because of preliminary data, security classification, or other reasons. Also includes conference proceedings with either limited or unlimited distribution.

CONTRACTOR REPORTS: Scientific and technical information generated under a NASA contract or grant and considered an important contribution to existing knowledge.

TECHNICAL TRANSLATIONS: Information published in a foreign language considered to merit NASA distribution in English.

SPECIAL PUBLICATIONS: Information derived from or of value to NASA activities. Publications include final reports of major projects, monographs, data compilations, handbooks, sourcebooks, and special bibliographies.

TECHNOLOGY UTILIZATION PUBLICATIONS: Information on technology used by NASA that may be of particular interest in commercial and other non-aerospace applications. Publications include Tech Briefs, Technology Utilization Reports and Technology Surveys.

Details on the availability of these publications may be obtained from:

SCIENTIFIC AND TECHNICAL INFORMATION OFFICE

NATIONAL AERONAUTICS AND SPACE ADMINISTRATION
Washington, D.C. 20546